2016-03-01

Lineations and Structural Mapping of Io's Paterae and Mountains: Implications for Internal Stresses

Alexandra Anne Ahern
Brigham Young University

Lineations and Structural Mapping of Io's Paterae and Mountains:

Implications for Internal Stresses

Alexandra Anne Ahern

A thesis submitted to the faculty of
Brigham Young University
in partial fulfillment of the requirements for the degree of

Master of Science

Jani Radebaugh, Chair
Eric H. Christiansen
Ronald A. Harris

Department of Geological Sciences

Brigham Young University

March 2016

ABSTRACT

Lineations and Structural Mapping of Io's Paterae and Mountains:
Implications for Internal Stresses

Alexandra Anne Ahern
Department of Geological Sciences, BYU
Master of Science

Io, the most volcanically active body in the solar system, also has some of the tallest and steepest mountains. The mountains seem to be tectonic in origin, yet the methods of their formation have not been decisively constrained and their associations with volcanic paterae are yet unclear. We have compiled global spatial statistics on mountain dimensions and orientations, lineations attributed to structures, straight patera margins, and patera dimensions in order to better define their genetic relationships and the mechanisms forming each type of feature. Additionally, we have produced 4 regional structural maps of mountain complexes and have proposed tectonic histories.

Global statistics show that paterae and mountains and their associated lineations are more common at low latitudes and that lineations attributed to tectonics have preferred azimuths of 45° and 135°, whereas straight patera margins and azimuths appear more random. Additionally, tectonic lineations tend to cluster to those of similar types and are smaller when closer together. Mountains in general on Io are isolated, varied in size and shape, and have no significant geographic patterns in those variations. These results may indicate that global-scale processes are involved in forming Io's tectonic structures, but that the diversity of mountain characteristics and the collapse of paterae adjacent to mountain complexes may be more regionally controlled.

Mapping of the Hi'iaka, Shamshu, Tohil, and Zal regions has shown that Io's mountains reside in large, faulted-bounded crustal blocks, which have undergone modification through local responses of subsurface structures. Strike-slip motion along reactivated faults has led to the formation of both transpressional and transtensional features, creating tall peaks and low basins, some of which are now occupied by paterae. Subsurface structures play a large role in Io's mountain diversity.

Based on interpretation of statistical results and on our localized mapping, we propose that Io's mountains result from a combination of crustal stresses involving both global and local-scale processes. Multiple faults and fractures in a variety of orientations formed in Io's lithosphere, created over billions of years by stresses imposed by volcanic loading and tidal flexing. These faults have been progressively buried over time under multiple layers of volcanic material. Stresses continuing from loading and tidal massaging sometimes occur at oblique angles to pre-existing faults, reactivating them as reverse, normal, or strike-slip faults. Because of this, large, cohesive fault-bounded blocks have undergone both transpressional and transtensional modification. Further degradation of mountains has also occurred from extensive mass wasting, gravitational collapse, and erosion by sublimation and sapping of sulfur-rich layers within the crust.

This model of fault-bounded blocks being modified by continual stresses and local structural response accounts for the variation and patterns of mountain sizes, shapes, and

orientations, along with their isolation and interactions with other features. It presents an explanation for the influence of global and regional tectonics and a more detailed account of the formation of some of Io's remarkable mountains.

Keywords: Io, tectonics, volcanism, orogenesis, surfaces (satellites)

ACKNOWLEDGMENTS

This work has most definitely been a collaborative effort, with many great minds coming together. I would first like to thank my advisor, Jani Radebaugh, for teaching me how to work autonomously, how to let ideas evolve and grow, and for ensuring that I had opportunities to be involved in the planetary science community on many occasions. I also thank Eric Christiansen and Ron Harris for their willingness to sit for long periods of time to help me develop my ideas more fully and completely. I am also grateful for the statistical assistance and expertise of Shannon Tass.

My experience in the geology department at BYU has been rewarding and life-changing thanks to the great people I have associated with. The faculty instilled in me a love of the science and a curiosity that helped to fuel me during my graduate research. The students that studied along with me made the journey all the more enjoyable. A special thanks goes to all of those that started as classmates and field-trip buddies and are now lifelong friends.

I am especially indebted to my family—my parents and grandparents for their constant love and support and for teaching me hard work and a passion for science since a young age. My sister, Brooke, for living out these graduate years with me, suffering through and celebrating every achievement with me. My “Irish” friends throughout Utah that brought me back to the music that both sustained me and redefined me. And lastly, Kellie Woodfield, for helping me navigate through these years in every way and at all times.

I feel that this work is the sum of many great people and ideas coming together and I am truly grateful for all that have been on this journey with me through the past three years.

TABLE OF CONTENTS

LIST OF TABLES

LIST OF FIGURES

1. Introduction

From our earliest observations, Jupiter's moon Io has been an anomalous and dynamic world (Morabito et al., 1979; Smith et al., 1979; Strom et al., 1979; Anderson et al., 1996; McEwen et al., 1998; Cruikshank and Nelson, 2007; Perry et al., 2007; Spencer et al., 2007). Its surface is a colorful mosaic of active volcanic and tectonic features, created over time from the vast stores of internal heat available within the moon (Peale et al., 1979). This heat is generated by intense daily tidal massaging from Jupiter, a result of the Laplace resonance between the Galilean satellites that causes Io's orbital eccentricity to be non-zero (Peale et al., 1979; Yoder et al., 1979; Schubert et al., 1981, Segatz et al., 1988). Io's tidal heat is released through rapid resurfacing (Johnson et al., 1979; Blaney et al., 1995) and crustal overturn (Schenk and Bulmer, 1998; Schenk et al., 2001; Turtle et al., 2001; Jaeger et al., 2003). The average heat flow at the surface of Io is ~20-30 times that of Earth (O'Reilly and Davies, 1981; Veeder et al., 1994; Turcotte and Schubert, 2002; Veeder et al., 2004; Veeder et al., 2009; Veeder et al., 2011) and the average resurfacing rate is ~1-10 cm/year (Johnson et al., 1979; McEwen et al., 1989; Geissler et al., 1999). Io has no visible impact craters, supporting the idea that its surface is only a few million years old (McEwen et al., 1989; Geissler et al., 1999; McEwen et al., 2000). Its density (3.57 g/cm^3) and its tall, steep topography suggest that the moon as a whole is primarily composed of silicates (McEwen et al., 1989; Carr et al., 1998; Geissler et al., 1999), but chalcophile elements, sulfur allotropes, and fresh mafic lavas give Io's surface its distinctive red, black, and yellow surface colors (Sagan, 1979; Carr et al., 1998; Geissler et al., 1999; Kargel et al., 1999). Many of these have been erupted from plumes and fissures, or onto patera floors (Carr et al., 1998; Geissler et al., 1999; Lopes-Gautier et al., 1999; Davies et al., 2001; Radebaugh et al., 2001).

Paterae, defined on Io as volcano-tectonic depressions, are some of the moon's most ubiquitous surface features, resembling terrestrial calderas and often having active lava flows on their floors (Carr et al., 1998; Radebaugh et al., 2001). Io also boasts some of the tallest and steepest mountains in the solar system (Schenk et al., 2001; Turtle et al., 2001; Jaeger et al., 2003; Turtle et al., 2007), supported by a crust composed of interlayered mafic silicates and sulfur compounds (McEwen et al., 1998; Schenk and Bulmer, 1998). Their structures are complex and variable and are absolutely key to our understanding of crustal processes on Io (Carr et al., 1998; Schenk and Bulmer, 1998; Schenk et al., 2001; Turtle et al., 2001; Jaeger et al., 2003; Turtle et al., 2007).

It is likely that Io's continual supply of internal heat and resultant volcanism play a role in its crustal evolution and deformation (Schenk and Bulmer 1998; Schenk et al., 2001; Jaeger et al., 2003). However, it has been unclear whether crustal stresses and modifications are generated on global or regional scales. Paterae and mountains are globally distributed and are among Io's most distinguishable volcanic and tectonic features (Carr et al., 1998; Radebaugh et al., 2001; Schenk et al., 2001; Jaeger et al., 2003). As such, they provide valuable insight into recent or current volcanic and tectonic processes operating within Io's crust (Jaeger et al., 2003). The relationships of these two features to each other, as well as the processes forming them, are still not well understood (Radebaugh et al. 2001; Jaeger et al., 2003). In this study, the mountains and paterae of Io have been examined at global and local scales to begin to determine the relative influences of global and regional stress fields and possible tectonic links between these two classes of features.

2. Background

Mountains

Despite Io's persistent volcanic activity, its ~135 reported mountains (Turtle et al., 2001; Turtle et al., 2007) are, with very few exceptions, classified as tectonic rather than volcanic in origin (Schaber, 1982; Nash et al., 1986; Carr et al., 1998; Schenk et al., 2001; Turtle et al. 2001). They lack distinguishable vents, calderas, or flows coming from their summits (Turtle et al., 2001) and are blocky and steep-sided, rather than conical. Ionian mountains have been defined by Schenk et al. (2001) as features of positive relief and measureable size higher than 1 km, not solely created by erosional processes. Schenk et al. (2001) measured the average mountain height to be 6.3 km, with Io's highest peak, Boösaule Montes (Fig. 1a), rising 17.5±3 km above the surface. They also measured the average length and width of mountains to be 158 km and 80 km, respectively, and the average area to be ~12,080 km^2. Mountains comprise 3% of Io's total surface area (Schenk et al., 2001).

The Voyager 1 and 2 spacecraft first observed Io's mountains up close, imaging the moon as a whole at ~0.5-20 km/pixel and its sub-Jovian hemisphere and south pole at < 0.5 km/pixel (Smith et al., 1979). Initial studies from Voyager images suggested that the mountains, several taller than Everest, were evenly distributed in both latitude and longitude and were tectonically-modified crustal blocks, rather than volcanoes, as was predicted (Smith et al., 1979; Carr et al., 1998). There was no pattern or alignment of mountains to suggest that a global tectonic regime, such as terrestrial plate tectonics, could be responsible for them (McEwen et al., 1989; Schenk et al., 2001; Turtle et al., 2007). The Solid State Imaging (SSI) camera aboard Galileo also imaged Io's surface from 1996-2002, making the mountains one of its main targets (McEwen et al., 2000). SSI data showed that mountains and paterae were often adjacent to one

another and many interpreted this to indicate that they could be genetically related (Radebaugh et al., 2001; Jaeger et al., 2003; Radebaugh 2005). Higher-resolution imaging by SSI also showed the diversity of Io's mountain morphologies, along with smaller-scale tectonic and mass wasting features (McEwen et al., 2000).

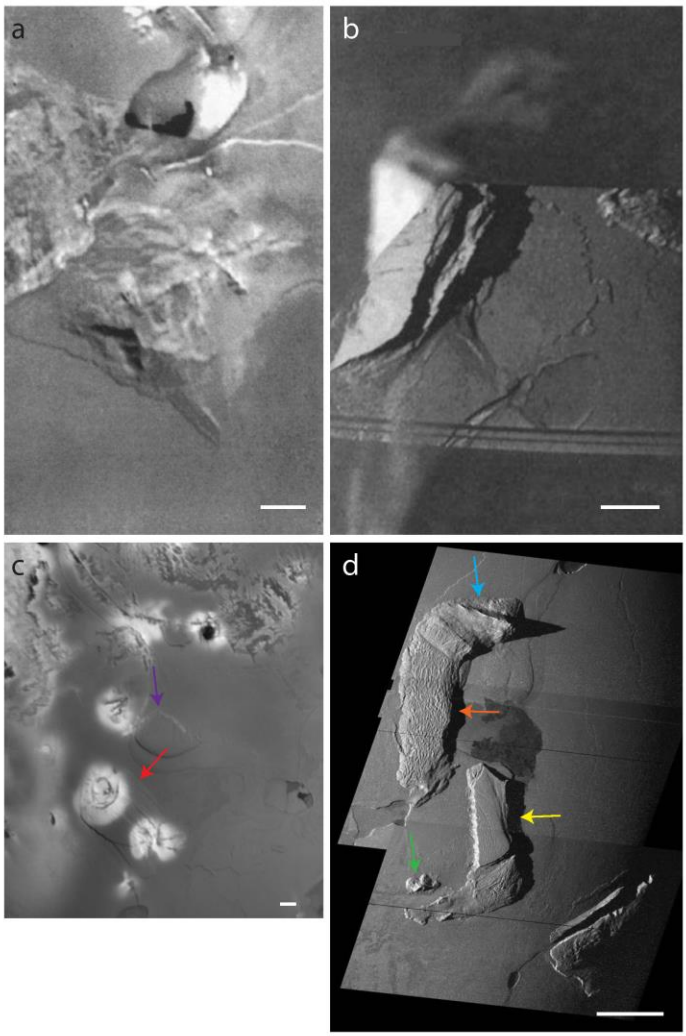

Figure 1: Examples of mountain diversity on Io. (a) Boösaule Montes, South (10°S, 271°W) has been designated as the type example of a massif and was measured at 17.3 ±3 km (Schenk et al., 2001), making it the tallest mountain on Io. Its summit is rugged and complicated and a cross sectional view asymmetrical. Voyager image (1.3 km/pixel). (b) Mongibello Mons (22°N, 67°W) stands at a height of 8.5 km. Its clear linear rises and planar sides have designated it as a ridge (Schenk et al., 2001). Galileo image (0.3-3.8 km/pixel). (c) Ethiopia Planum (44°S, 27°W, purple arrow) and Pan Mensa (49°S, 33°W, red arrow) are both examples of a mesa and plateau, respectively. Ethiopia Planum is defined by its smooth, flat, elevated plain and Pan Mensa is also elevated but has a more rugged, striated flat surface. Voyager image (1.2 km/pixel). (d) Hi'iaka Montes (3.5°S, 79.5°W) contains several examples. Its lineated plateaus are indicated by the orange and yellow arrows, while its steep, linear ridges on the north end are marked by the blue arrow. Additionally, the green arrow shows Hi'iaka Montes (west), which is dominated a single sharp point and thus is interpreted as a peak. Galileo image (250 m/pixel). North in all images is up. All of the scale bars represent 50 km.

The morphologies of mountains on Io vary greatly (Fig. 1). The majority appear as isolated islands that climb suddenly and steeply out of the surrounding smooth, volcanic plains. Others have scalloped margins eroded from possible sapping of sulfur-rich crustal layers or are surrounded by debris aprons. Many bounding scarps can be interpreted as either tectonic, erosional, or a result of gravitational collapse (Schenk et al., 2001). Io's mountains possess lineations, striations, and troughs that could have been created by arching or detachment during uplift or by mass movement (McEwen, 1985; Carr et al., 1998; Schenk et al., 2001). Carr et al. (1998) and Schenk et al. (2001) compiled global catalogs of mountains from Voyager and Galileo data. They identified mountains through low-illumination-angle terminator images, twilight observations, limb profiles and stereo images, which in total cover 95% of Io's surface. Schenk et al. (2001) then divided Io's mountains into 5 categories based on summit morphologies (Fig. 1): mesas, plateaus (Fig. 1c, 1d), peaks (Fig. 1d), ridges (Fig. 1b, 1d), and massifs (Fig. 1a). Some mountains received two morphological assignments if their summits represented multiple categories. These characterizations were only made for areas with coverage of <200 m/pixel, but have nevertheless been helpful in aiding our understanding of the diversity of mountain morphology on Io.

Mountain distributions and their relationships to volcanic centers have long been discussed. Carr et al., (1998) did not find a correlation between mountains and volcanic hot spots. However, Schenk and Hargitai (1998) reported a longitudinal anticorrelation between mountains and volcanic centers, results since validated in other research (McKinnon et al., 2001; Schenk et al., 2001; Kirchoff et al., 2009; Kirchoff et al., 2011). Mountains seem to be slightly more densely clustered at lower latitudes (Schenk et al., 2001) and show two broad concentrations around 65°W and 265°W, roughly antipodal from one another (McEwen and

Soderblom, 1983; Schenk et al., 2001; Kirchoff et al., 2003; Kirchoff and McKinnon, 2005). These concentrations are 90° offset from two clusters of volcanic centers reported by Radebaugh et al. (2001) and Schenk et al. (2001). The global anticorrelation between mountains and volcanic centers may suggest that heat flow in the crust is higher in the areas where volcanic centers are concentrated (Radebaugh et al. 2001), while 90° from those areas there exists colder, thicker, and more brittle crust more suitable for the formation of mountains through tilted crustal blocks (Schenk and Bulmer, 1998; Schenk et al., 2001; Turtle et al., 2001; Jaeger et al., 2003; Kirchoff et al., 2009).

A number of possible formation mechanisms for Io's mountains have been discussed (Carr et al., 1998; Schenk and Bulmer, 1998; Schenk et al., 2001; Jaeger et al., 2003; Turtle et al., 2001; Turtle et al., 2007). McEwen et al. (1985) postulated early on that Io's crust was experiencing basin-and-range style extension, with high heat flow below a thin lithosphere, magmatism, and topographic swelling. Keszthelyi et al. (1999) proposed that the lithosphere of Io is negatively buoyant on a dense, partially molten upper mantle and that mountains are crustal blocks associated with remixing of the lithosphere into the mantle. Others have linked tidal massaging to the formation of tectonic features. Bart et al. (2004) concluded that fields of ridges are directly linked to crustal stresses predicted for tidal flexing, suggesting that a global input of tidal stresses may be overprinting local stress fields. This model is challenged by the fact that many tectonic features on Io suggest longer-lived processes than the diurnally changing tidal stress fields, unless given fractures undergo diurnal reactivation and continued slip. Non-synchronous rotation would bring additional and differential stresses to Io's crust because the sub-Jovian side would continue to rotate while Io's tidal bulge faced Jupiter (Bart et al., 2004). The ephemeral nature of crustal stress due solely to tidal massaging would be unlikely to form mountains directly without the input of

stresses from longer-lived processes. Still others have proposed that local convective upwelling, due to global tidal heating, may be generating asthenospheric diapirs that rise and dome the surface, creating local horizontal compressive stresses sufficient for mountain formation (Jaeger et al., 2003). This process may be similar to those forming the chaos terrains of Europa (McKinnon et al., 2001). However, the resurfacing rate on Io seems uniform over appropriate timescales, and the chaos model would suggest that resurfacing rates would fluctuate both temporally and spatially (Jaeger et al., 2003).

One of the most widely accepted models for mountain formation on Io, and the one that forms the groundwork for this study, was put forth by Schenk and Bulmer (1998). They linked horizontal shortening in the crust to vertical compressive stress generated by constant volcanic resurfacing. In essence, they suggested that Io was building successive global crustal shells of volcanic materials and shortening its radius each time a new shell loaded the surface. Then, as horizontal compressive stresses became high enough to exceed the compressive strength of rock in the lithosphere, mountain blocks popped up along high-angle reverse faults (Schenk and Bulmer 1998; Turtle et al., 2007). In some areas, crustal anisotropy, localized fracturing, or nearby volcanic activity could have triggered failure (Schenk and Bulmer, 1998). This model has joined volcanism and tectonism in a way that gives Io its own, unique form of tectonics. It further emphasizes the need to understand the relationship of the mountains and nearby volcanic features both structurally and genetically. Exploration into these topics may yield greater insight into crustal properties and subsurface structure and mechanics, which would shed light on Io's formation and evolution.

Paterae

Features classified as volcanic centers on Io include single vents, fracture vents, flow fields, shield volcanoes, and paterae (Schenk et al., 2001; Williams and Howell, 2007; Kirchoff

et al., 2011). Of all of the features classified as volcanic centers, the majority are paterae, numbering over 400 (Radebaugh et al., 2001; Barth and Radebaugh, 2010; Williams et al., 2012). Often compared to terrestrial calderas, these depressions are attributed to collapse into a partially drained magma chamber or into voids left by the sublimation of layers of sulfur frosts within the crust (Radebaugh et al., 2001; Keszthelyi et al., 2004). Paterae have steep walls and flat floors that are often covered or partially covered by relatively young lava flow deposits (Radebaugh et al. 2001; Williams et al., 2012). The average patera effective diameter (diameter of a circle having the same area as the patera) from a database of 417 paterae is 41 km (Radebaugh et al. 2001).

Hamilton et al. (2013) reported that paterae tend to be uniformly distributed where active volcanism is driving hotspots apart, except in the more northern regions where they are randomly distributed. Paterae are found slightly more frequently between 25°S and 25°N latitude and cluster around 330°W and 150°W longitude (Radebaugh et al., 2001), as do the total volcanic centers (Lopes-Gautier et al. 1999). These longitudinal clusters are 30-60° offset from predicted locations of maximum surface heat flux along Io's tidal axes, suggesting that Io may be rotating slightly faster than its synchronous rotational speed (Radebaugh et al., 2001) or that magma is able to travel laterally by way of local subsurface structures (Hamilton et al. 2013). Volcanic centers, including paterae, are longitudinally anti-correlated with mountains (Schenk et al., 2001; Jaeger et al., 2003; Kirchoff et al., 2011; Hamilton 2013), which Kirchoff et al. (2013) have said indicates independent formation processes between the two types of features. However, 13% of paterae are adjacent to at least one mountain, while 42% of mountains have at least one adjacent patera (Radebaugh et al., 2001; Jaeger et al., 2003). Kirchoff et al. (2013) have also noted

positive correlations between mountains and volcanic center distributions. This may imply that there are structural links between some mountains and their adjacent paterae.

Paterae are not always round or sub-round, as is often the case with terrestrial calderas. Instead, many have straight, sharp portions to their margins (Radebaugh et al. 2001). It is possible that the straight edges of paterae indicate tectonic elements in their formation or genetic relationships to adjacent mountains, but this is yet unclear. It is also possible that the amount of patera floor coverage by lava could indicate the presence of subsurface structures acting as magma conduits in areas of current or recent tectonic activity.

In this study, we investigate possible relationships between mountains and paterae by looking at spatial relationships between them and the structural features that may be related to their formations. We look at the relationships between mountains and paterae, specifically, where previous statistical analyses between paterae and mountains have included all volcanic centers (Carr et al., 1998; Kirchoff et al., 2011; Hamilton et al., 2013; Kirchoff et al., 2013). Additionally, paterae with possible structural influence are identified and their relationships to mountains are characterized to determine the extent of tectonic controls on their collapse. This study should shed light on the processes forming mountains and paterae on Io, the way the crust has been modified by tectonic activity, and possible stress inputs to Io's crust.

3. Global Spatial Statistics

Methods

In order to investigate the extent, effects, and sources of stress in Io's crust, we have performed spatial analyses on its mountains, structural lineations, and paterae. Specifically, we

looked at lineations associated with each feature, feature sizes, and feature locations. We mapped all lineations and features for this spatial study (Fig. 2, Fig. 3) in ArcGIS using the Io merged, north pole, and south pole mosaics as base maps under the Io 2000 Geographic Coordinate System and North Pole and South Pole projections (Williams et al., 2012). These mosaics combine Galileo color data with the high-resolution monochrome mosaic of both Voyager Imaging Science Subsystem (ISS) and Galileo SSI monochrome images. The merged mosaic is a simple cylindrical map projection centered on 0° longitude. The global resolution ranges from 1-10 km/pixel on or near the equator and up to 10 km/pixel in the low-resolution longitudinal band near 50° W, and there is no coverage within 5 degrees of the north pole (NASA Planetary Photojournal, 2007; Williams et al., 2012). Although there are select locations of Io imaged at higher resolutions, we mapped lineations and features for our statistics on the merged mosaic for global continuity.

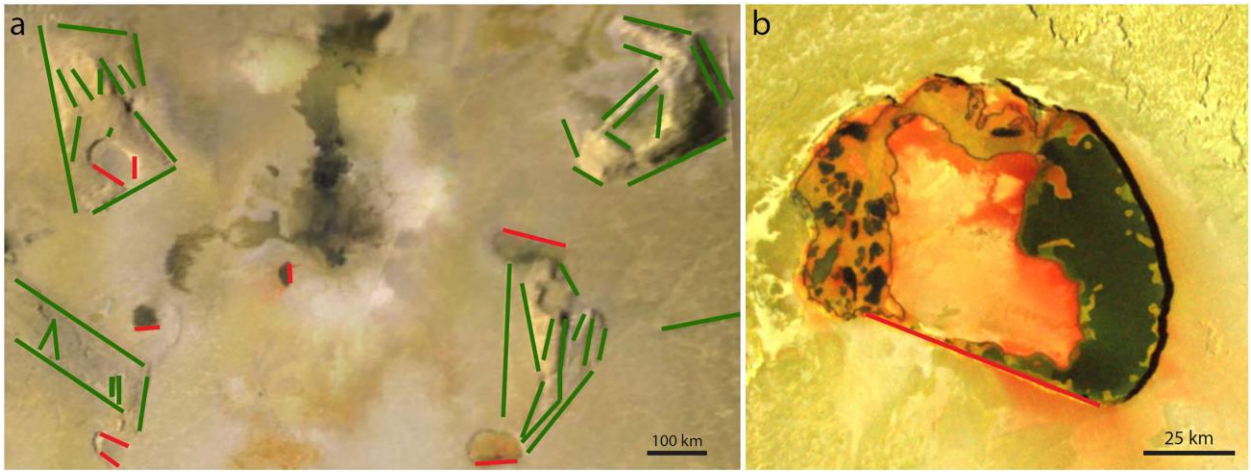

Figure 2: Examples of lineations identified in this study. (a) Structural (green) and patera edge (red) lineations traced over an image of the region surrounding Amirani (~25°N, 114°W) taken from the merged mosaic. (b) Straight margin of Tupan Patera (18.5°S, 141°W), type example of a patera edge lineation for this study.

We identified and measured lineations across the surface of Io and divided these into two categories—structural lineations and patera edge lineations, examples of which are given in Fig. 2. Structural lineations refer to any features interpreted as faults, fractures, or folds—thus

features that have formed as a result of tectonism. Patera edge lineations are defined as straight margins of paterae and were considered alongside, but separate from, structural lineations because of their possible tectonic origins (Fig. 2b). The azimuths and lengths of all identified lineations were calculated in ArcGIS using the COGO Toolbox (Fig. 3). In addition to lineations, we measured the long axes of paterae and calculated their azimuths and lengths in ArcGIS. We also measured lengths, widths, and areas in ArcGIS of 82 mountains using polygonal shapefiles to calculate areas. Of Io's ~135 mountains (Turtle et al., 2007), we were only able to discern 82 well enough to find boundaries between them and the surrounding plains at the resolutions of the global mosaic. However, this method may lead to greater refinement of mountain dimensions in the future. We updated the previous catalog of paterae by Barth et al. (2010) by using high resolution images to find additional paterae and reclassify paterae that were previously labeled as mountains. Paterae in the current updated catalog number 473 in total across the surface of Io.

With this data, we first tested our measurements for distributional patterns by looking at the clustering of lineations and lineation characteristics (length and azimuth) in 16 sectors of equal area across Io. Then, global distributional patterns were explored for mountain sizes, patera sizes, and patera floor lava coverage measured previously by Barth et al. (2010).

It is visually apparent that some features are clustered at various locations and scales (Fig. 3). We tested for spatial randomness—whether our data points were in fact clustered, or were random or uniform—using the *G* and *K* functions. The *G* function is a nearest neighbor distance function that quantifies spatial interaction between features. It gives the proportion of the number of data points in the set of distances up to a given cutoff, *r*, to the total number of points expected under complete spatial randomness (CSR). To achieve bounds for CSR, a series of runs through the function are made with parameters randomized. We performed 100 runs

through both the *G* and *K* functions to determine the range in which we would reasonably expect our data to plot under CSR. For a clustered pattern, features or measurements would be closer to each other than expected from CSR and therefore plot above CSR. For a uniform pattern, they would be farther apart than expected and plot below CSR (Zhukov, 2010). The *K* function is also a distance function between features but looks beyond nearest neighbors. It shows interactions between points by looking at the cumulative number of features around all others within a certain radius, *r*. Like the *G* function, the *K* function is compared to a predicted range of CSR (Funk, 2011). In most of the analyses we used great circle distances of latitude and longitude points but calculated the *G* and *K* functions using simple Euclidean distances.

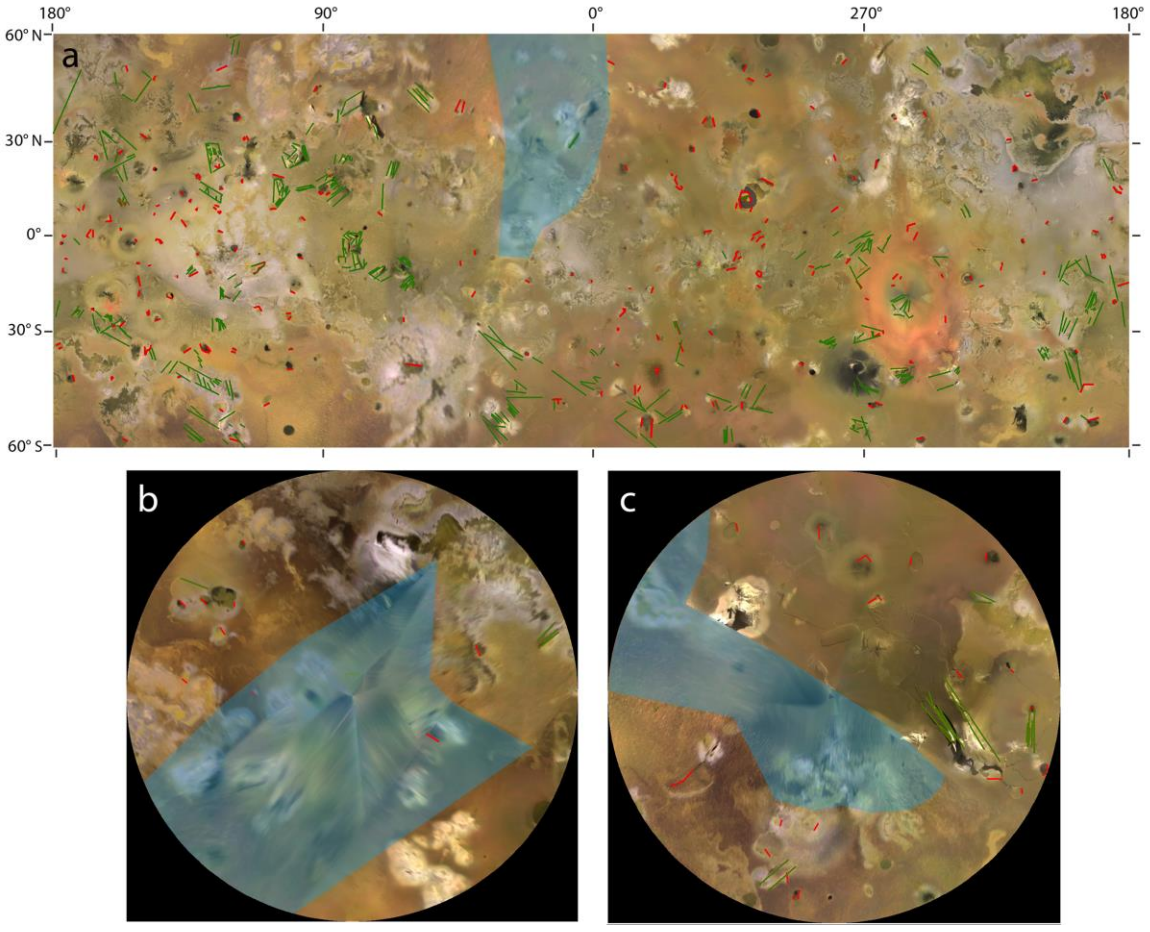

Figure 3: Global lineations. (a) Structural lineations (green) and patera edge (red) lineations traced on the merged mosaic image as interpreted in this study. (b) Lineations traced on the north pole mosaic as interpreted in this study. (c) Lineations on the south pole mosaic as interpreted in this study. Blue shaded regions indicate areas of lower resolution.

Additionally, we looked at conditional marked moments of length and azimuth measurements, or the conditional mean and variance of the lengths and azimuths of linear measurements at distances *r* away from other lineations. These tests are used to indicate whether similar length or azimuth values tend to cluster. We did this by fixing measurement locations and varying lengths and azimuths randomly for 100 scenarios. This provides an average, with some variation for randomness, that the lengths and azimuths of our data are measured against in order to detect patterns at great circle distances in 50 km intervals away from each feature. The number and character of each feature is analyzed along each given great circle, rather than in a summative area covered by all previous great circles. If points plot within the bounds of variance around the mean, then we can conclude that there is no pattern, but rather that lengths and azimuths vary randomly with location. If they plot above or below the bounds we generated, then some locational pattern exists for the lengths or azimuths of our lineations.

Lastly, we used a nonparametric circular-linear correlation to correlate the azimuths and lengths of linear features since azimuth is an angular measure and length is linear. To do this, each azimuth value was converted to a ranked circular variable, β_i, by:

$$\beta_i = \frac{2\pi(r_i)}{n}$$

where n is the total number of pairs of azimuths and lengths and r_i is the corresponding circular rank of the azimuth measurements. We then calculated T_c and T_s:

$$T_c = \sum_{i=1}^{n} x_i \cos(\beta_i)$$

$$T_s = \sum_{i=1}^{n} x_i \sin(\beta_i)$$

where x_i is the rank of the length measurements. Finally, we calculated the correlation coefficient, R, given by:

$$R = \frac{24\left(T_c{}^2 + T_s{}^2\right)}{n^2(n+1)} \sim \chi^2 \; as \; n \to \infty$$

using the values we obtained for T_c and T_s above. To scale to traditional R-values between 0 and 1, transformations were performed for when n is even and odd, respectively, given by:

$$a_n = \frac{1}{1 + 5cot^2\left(\frac{\pi}{n}\right) + 4cot^2\left(\frac{\pi}{n}\right)}$$

and

$$a_n = \frac{2sin^4\left(\frac{\pi}{n}\right)}{(1 + cos\left(\frac{\pi}{n}\right))^3}$$

We used values obtained for a_n to calculate a scaled correlation, given by:

$$D_n = a_n\left(T_c{}^2 + T_s{}^2\right)$$

as given by Tu (2015).

The last step in our spatial statistics was to test the relationships between straight patera margins and mountain locations to determine if they could be genetically related. We used three different tests—the Equality Function, an independence test, and a random labeling test. The Equality Function measures how similar events are at different distances. Values greater than 1 indicate that there is some kind of relationship; that is, features that are closer together tend to be of a similar type. The independence test looks at whether the individual point location-determining processes are independent of one another, assuming a null hypothesis that the two processes, and therefore features, are spatially independent of each other. Finally, a random

labeling test compares the locations of data points of the same type with random reassigned locations. Predicted bounds were again generated for these tests using 100 scenarios in which parameters determining location designations were randomly varied. These help us to understand the interaction of mountains with each other and with paterae that may be exhibiting tectonic influence.

The spatial statistics and feature identifications conducted in this study build on geologic mapping and measurements made on the Io ArcGIS Project by Williams et al. (2012), a lineation study by Radebaugh et al. (2011), mountain spatial measurements by Schenk et al. (2001), a comprehensive patera study by Radebaugh et al. (2001), and spatial analyses of mountains and volcanic features conducted by Kirchoff et al. (2009), Kirchoff et al. (2011), and Hamilton et al. (2013). Areas of low resolution may affect the confidence level of some of the statistical results presented, and those are identified and accounted for. Nevertheless, Io has sufficient image coverage currently such that our results are still statistically significant. Given higher resolution images of low resolution areas, it is expected that the amount of uncertainty surrounding our results would decrease.

Results

Structural Lineations.

There are 353 features identified as structural lineations located on the surface of Io (Fig. 4). The lengths and azimuths of the structural lineations are shown in 16 sectors of equal area in Fig. 5.

Most structural lineations occur between 60° S and 30° N latitude, and those between 15° S and 0° are shorter than at other latitudes (Fig. 5). It is possible that identification of lineations as a whole, and discernment between small lineations, is facilitated by the higher resolutions

available in the lower latitudes, but with the amount of available coverage of Io's surface these patterns can still be said to exist, especially locally. There does not seem to be a statistically significant latitudinal pattern of azimuths of structural lineations (Fig. 5), which characteristic would be least likely to be affected by gaps in resolution. The highest frequency of structural lineations longitudinally occurs between 180° W and 240° W. Lengths and azimuths do not appear to show longitudinal patterns, except for a cluster of lineations with azimuths oriented at roughly 130° between 300° W and 330° W.

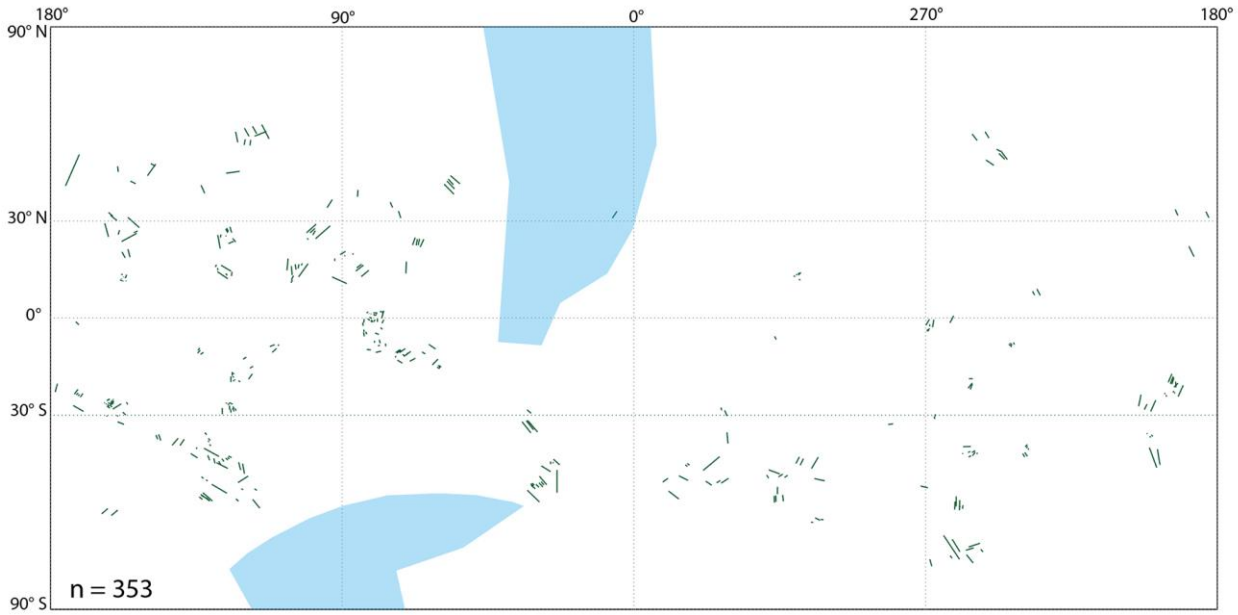

Figure 4: Structural lineation traces. Latitude and longitude locations and approximate orientations of all structural lineations identified in this study. Blue shaded regions indicate areas of lower resolution.

The patterns visible in Fig. 4 reveal that structural lineations exhibit clustering by location, and we have confirmed this statistically through the *G* and *K* functions (Fig. 6). In both cases, the observed values, or those we have measured for our lineations, far exceed the predicted bounds of CSR as shown by the gray bands. This indicates strong clustering of identified linear structures.

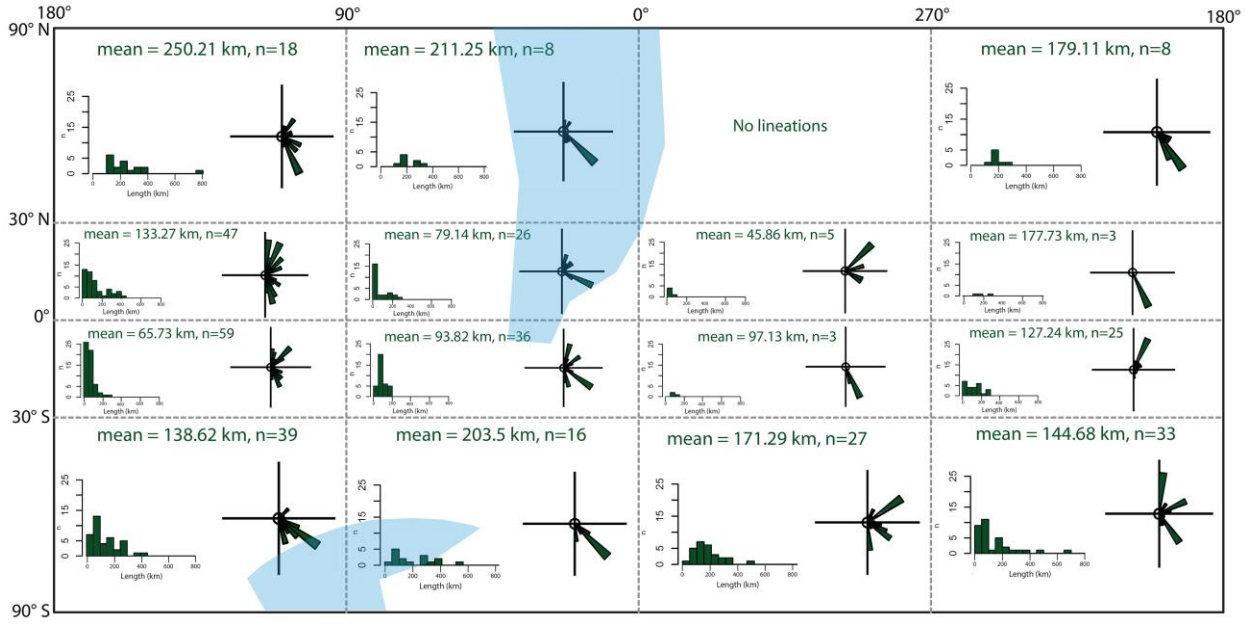

Figure 5: Structural lineation lengths and azimuths by sector. Longitude is measured in °W.

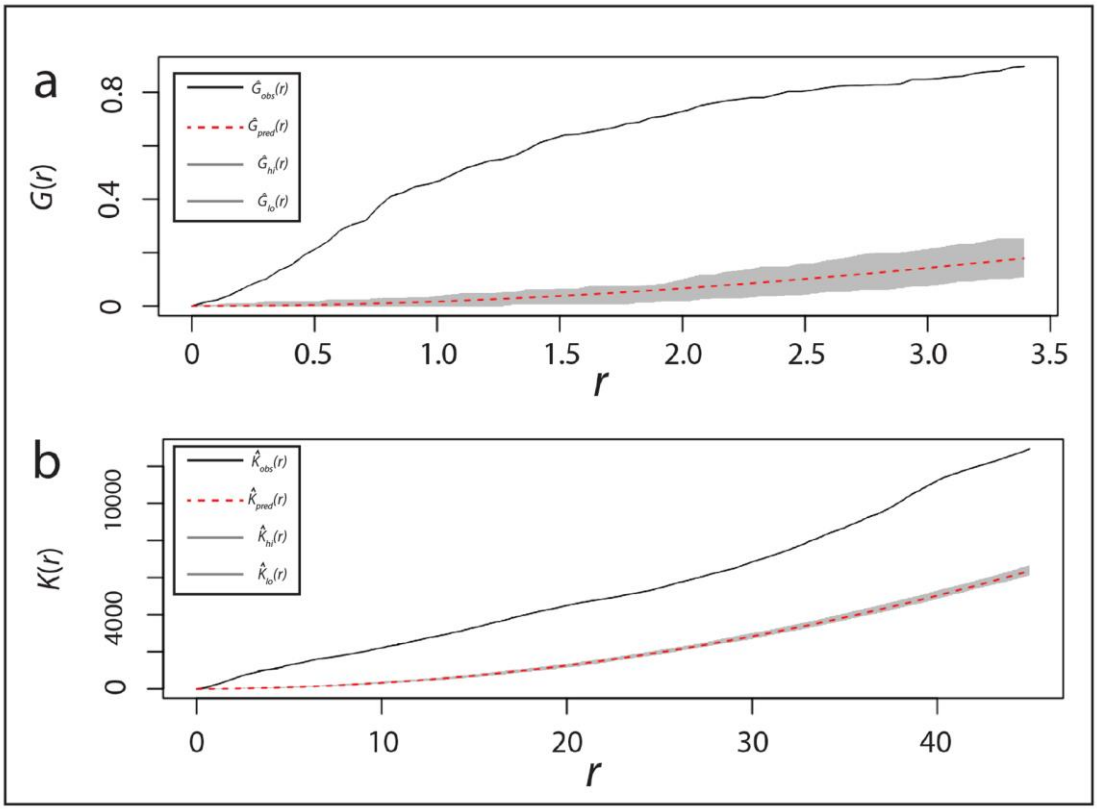

Figure 6: Comparison of *G* (a) and *K* (b) functions with structural lineation data. The predicted bounds of CSR of both functions are represented by gray shading, with the average predicted values for each function represented in the middle of those bounds by the red dashed line. Observed values for structural lineations are shown by the black line. Both functions indicate strong clustering of structural lineations.

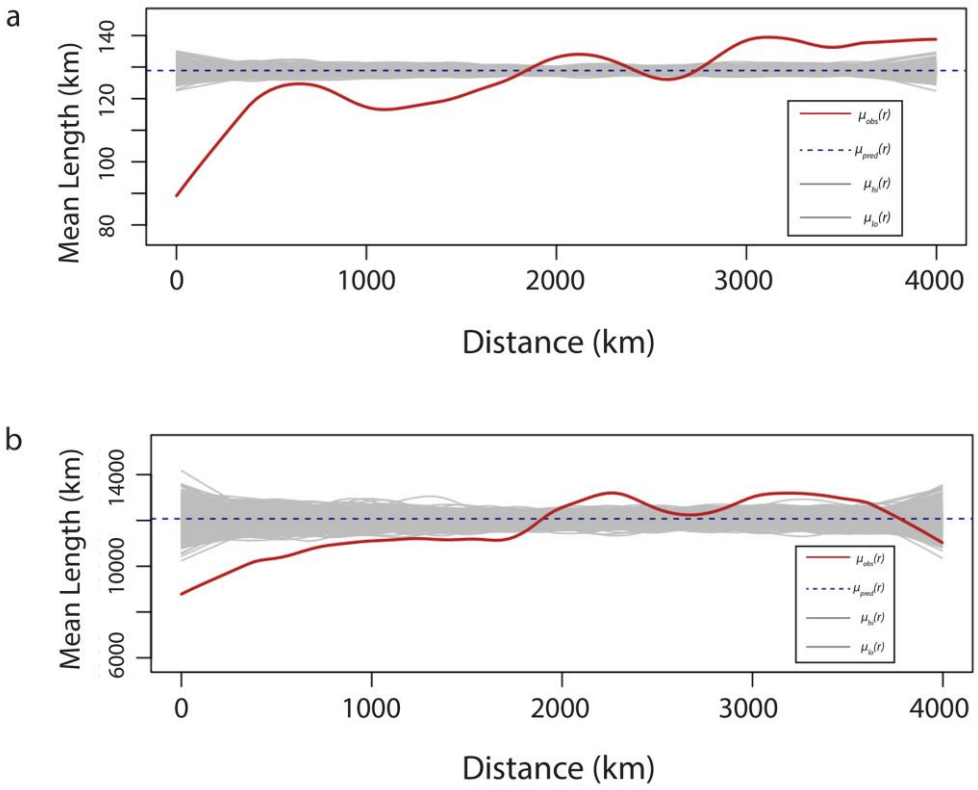

Figure 7: Conditional marked moments of structural lineations. (a) shows the conditional mean, with global average and its bounds indicated by the dashed blue line and the gray band, respectively. The red line indicates the values for the structural lineations in this study. (b) shows the conditional variance, with global average and its bounds indicated by the dashed blue line and the gray band, respectively. The red line indicates the values for the structural lineations in this study.

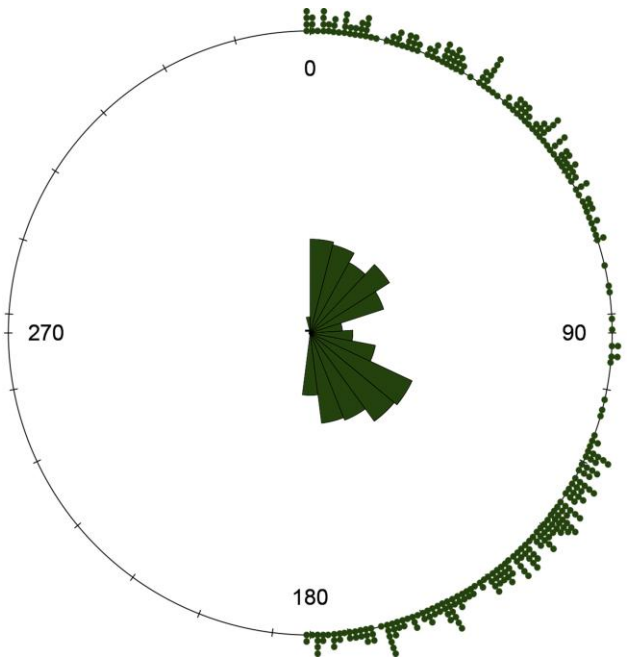

Figure 8: Rose diagram of structural lineation azimuths.

We then looked at conditional marked moments for the lengths of the structural lineations to see how far trends in the lineations propagate. The average length of structural lineations globally is ~130 km. Fig. 7a shows that lineations having neighbors within 500 km are much shorter than the global average, with mean lengths of 90-120 km. Those having neighbors within 2000 km are still shorter than the average, but not as short as those with very close neighbors. Once lineations are more than 3000 km apart, they tend to be longer than the global average lineation length. The maximum distance between any features on Io is half of the moon's perimeter, or 5722 km. Conclusions drawn about lineations at distances of 3000 km to 5722 km apart may not be as useful statistically, given that the low resolution areas will be encountered at some point measuring away from all lineations. Nevertheless, results from lineations of close neighbors are valid. The variations between lineation lengths, shown in Fig. 7b, have a similar pattern. Lineations with closer neighbors tend to have a smaller variance, and are therefore more similar in length, than lineations with neighbors farther away.

The azimuths of all structural lineations prefer orientations at 45° and 135° (Fig. 8). This suggests that a global stress field may play a role in the formation of structural features on Io. The 90° offset between orientation peaks may suggest one overall stress regime (with petals perpendicular to the directions of σ_1 and σ_2) or two different stress regimes occurring at different times from one another (with petals both indicating the direction of σ_1 for each stress regime). Variation in the azimuth angles of the structures may also be controlled by local subsurface structures, crustal anisotropies, or local volcanic activity.

Lengths and azimuths of the structural lineations do not appear to be related. From our calculations, we obtained a p-value for our null hypothesis of no relationship of 0.764, suggesting that the null hypothesis is valid and that there is no relationship between the lengths

and azimuths of structural lineations. This means that there is not likely one major stress regime responsible for creating the largest structural features globally on Io. Instead, orientations and lengths of tectonic features as a whole may be more complicated—they may controlled by multiple large-scale stress regimes and by local subsurface structure or crustal anisotropies.

Patera Edge Lineations.

We measured 306 patera edge lineations and analyzed them in the same way that we did structural lineations. 193 paterae, or 41% of the total paterae identified, have at least one straight margin (Fig. 9). Paterae with straight margins occur most frequently in the equatorial region, as do paterae themselves (Radebaugh et al., 2001). Longitudinally, straight patera margins occur most commonly between 180° W and 90° W and between 300° W and 0°. It is still possible to see large paterae even in low-resolution regions, and many paterae in these regions seem to have more rounded edges.

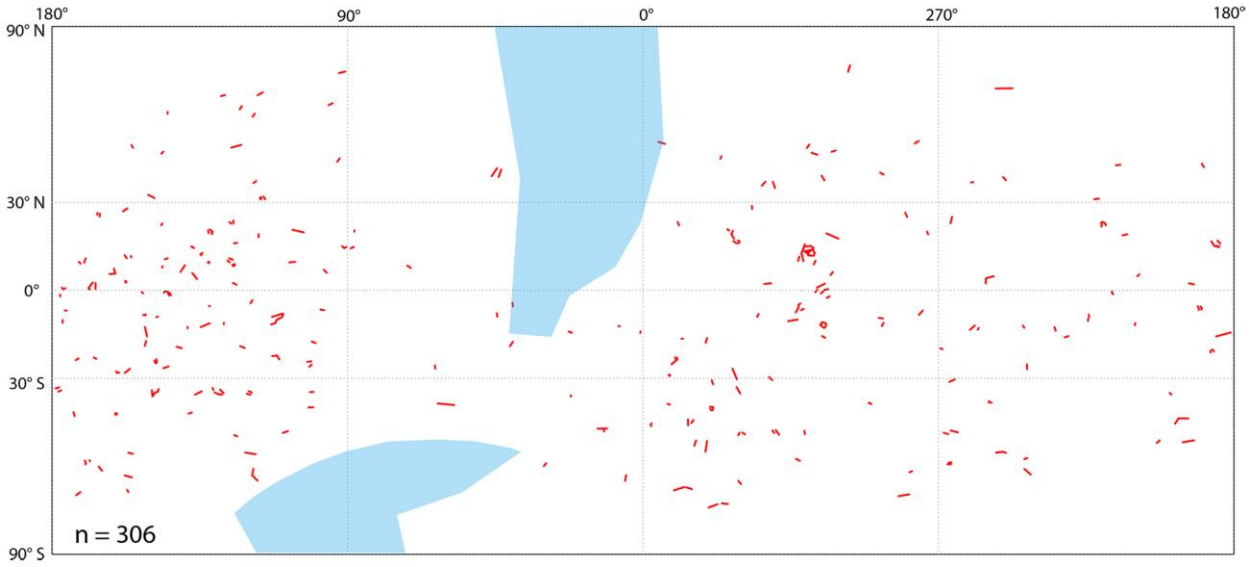

Figure 9: Patera edge lineation traces. Latitude and longitude locations and approximate orientations of all straight patera margins identified in this study. Blue shaded regions indicate areas of lower resolution.

Again, the global view of patera edge lineation seems to show clustering (Fig. 9), and again, this is confirmed by comparison with the *G* and *K* functions. Our results indicate strong clustering of straight patera margins (Fig. 10). Patera edge lineations have smaller average lengths than structural lineations overall; nevertheless, like the structural lineations, they are shorter than the average length in lower latitudes. This was verified by observing trends in the 16 sectors, as was done for structural lineations. Additionally, patera edge lengths are also shorter than the global average when they have neighboring patera edges within 2000 km (Fig. 11a). The variance, however, is not statistically different from what we would expect if there were no relationship between the locations of lineations and length (Fig. 11b).

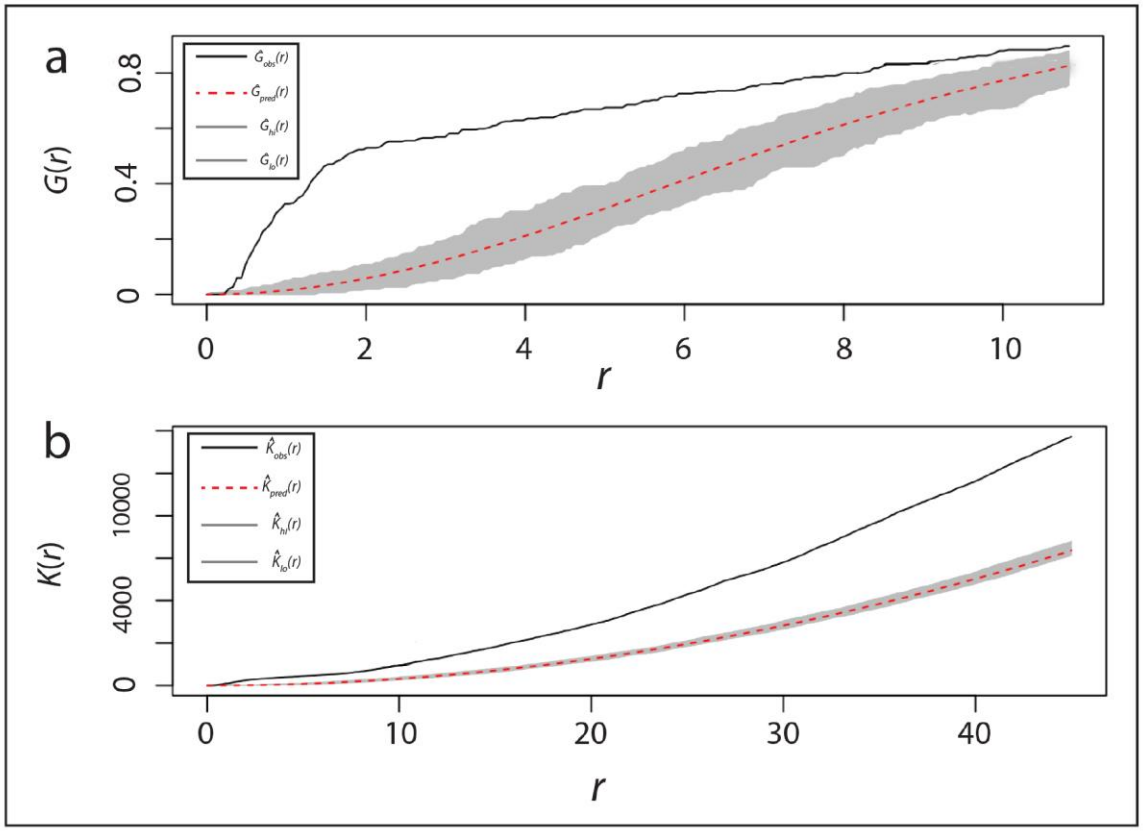

Figure 10: Comparison of *G* (a) and *K* (b) functions with patera edge lineation data. The predicted bounds of both functions are represented by gray shading, with the average predicted values for each function represented in the middle of those bounds by the red dashed line. Observed values for structural lineations are shown by the black line. Both functions indicate strong clustering of patera edge lineations.

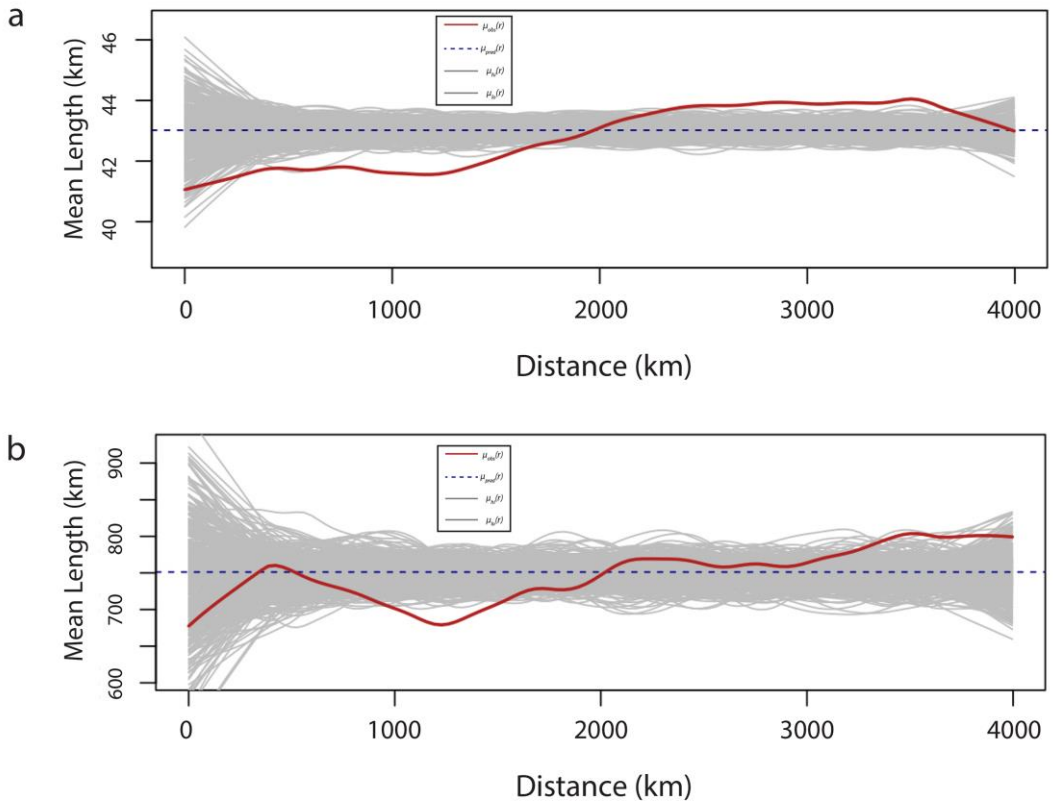

Figure 11: Conditional marked moments of patera edge lineations. (a) shows the conditional mean, with global average and its bounds indicated by the dashed blue line and the gray band, respectively. The red line indicates the values for the patera edge lineations in this study. (b) shows the conditional variance, with global average and its bounds indicated by the dashed blue line and the gray band, respectively. The red line indicates the values for the patera edge lineations in this study.

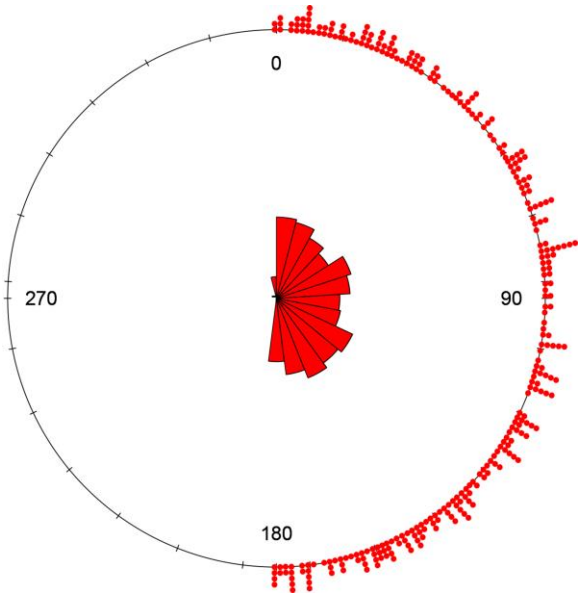

Figure 12: Rose diagram of patera edge lineation azimuths.

Compared to structural lineations, patera edge azimuths have no significant preferred orientations (Fig. 12). This could indicate that collapse within paterae along straight margins may not be caused by a global tectonic regime, but rather is governed by localized stresses or local subsurface structures.

There also seems to be no relationship between the location of a patera edge lineation and its azimuth. However, using the same nonparametric circular-linear correlation between length and azimuth, we obtained a p-value of 0.052. This suggests that we cannot reject the null hypothesis of no relationship between the lengths and orientations of straight patera edges, but with the small and inconclusive p-value, further investigation into the possibility of a relationship may be necessary.

Mountain Spatial Statistics.

The 82 mountains that were measured in this study do not possess an obvious distribution pattern, but mountain widths and areas are smaller at low latitude regions (15°S to 15° N) and poleward of 60° S (Fig. 13). There seem to be no patterns in mountain lengths, widths, or areas by longitude. There also does not appear to be any statistically meaningful patterns relating the distance between mountains and their lengths, widths, or areas. In sum, mountains are isolated, varied in size and shape and have no significant geographic patterns in those variations. This may mean that some type of global stress regime causes mountain formation, but that response to global stresses varies due to local subsurface features. These statistics are limited by gaps in resolution that have prevented us from decisively identifying or constraining the dimensions of the remaining ~53 mountains as identified by Schenk et al. (2001) and Jaeger et al. (2003).

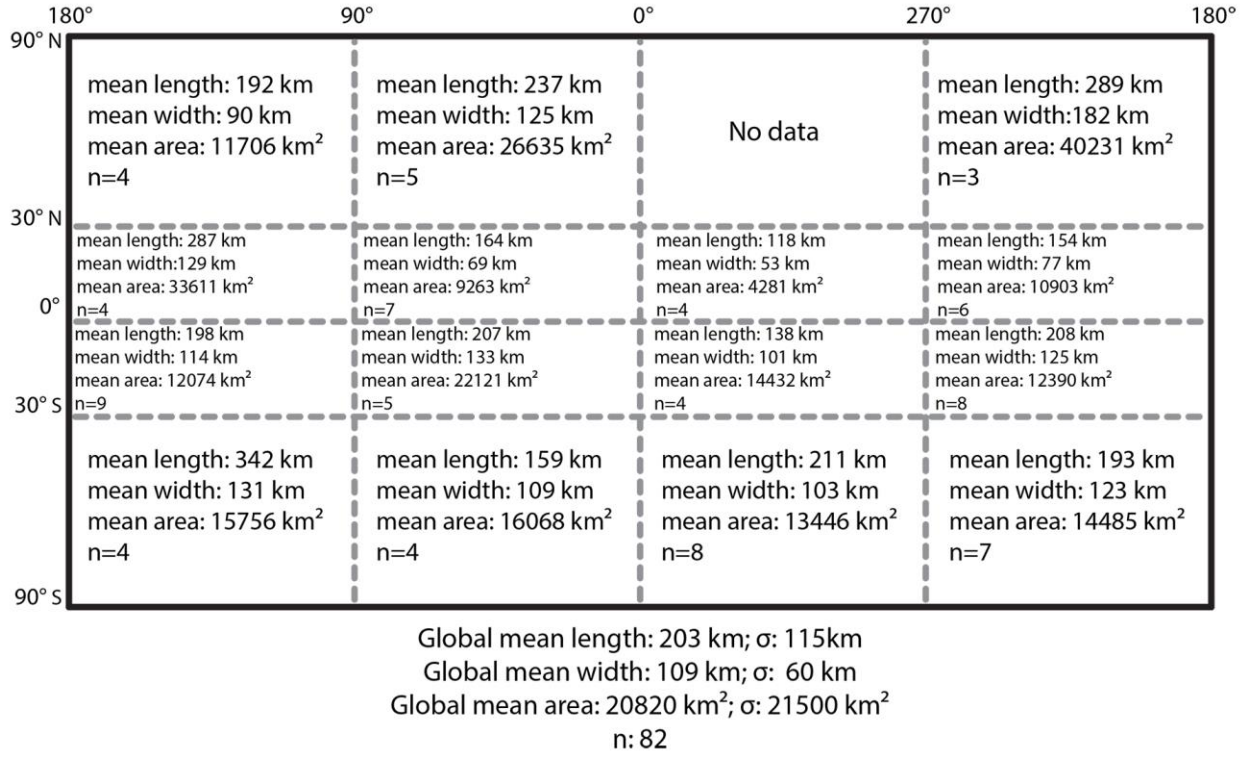

Figure 13: Mountain size statistics by sector. Longitude is measured in °W.

Patera Spatial Statistics.

Our results support the findings of Radebaugh et al. (2001) that the majority of paterae are found at low latitudes (with 56% between 30°S and 30°N) when considered in equal areas. Although they occur more frequently, paterae in this latitudinal band seem to be smaller than the global average (Fig. 14).

We also observed a slight clustering of paterae around 330°W and 150°W close to Io's sub-Jovian and anti-Jovian faces, as also seen by Radebaugh et al. (2001). Others have noted concentrations of general volcanic centers in these areas as well, offset 90° from maximum mountain concentrations (Schenk and Hargitai, 1998; Lopes et al., 2001; McKinnon et al., 2001; Schenk et al., 2001; Kirchoff et al., 2011; Hamilton et al., 2013). There does not seem to be a longitudinal pattern of patera sizes (perimeters or areas) based on variations between sizes in

each of the 16 sectors. However, between 260°W and 0° more paterae occur that have 50% or 100% floor coverage by young, still dark lava (Fig. 15)**.** This may coincide with more active regions of volcanism possibly associated with tidal stresses (Ross et al., 1990; Segatz et al., 1998; Tackley et al., 2001) or with subsurface structures allowing magma to migrate to the surface more easily in some regions than in others. Paterae with significant floor coverage do not seem to follow the same patterns as general hotspots across Io. Lateral movement of magma along subsurface structures could cause lavas to erupt onto patera floors that are not necessarily located along the same trends as hotspots, even though this magma is sourced from the same locations as that erupting at hotspots.

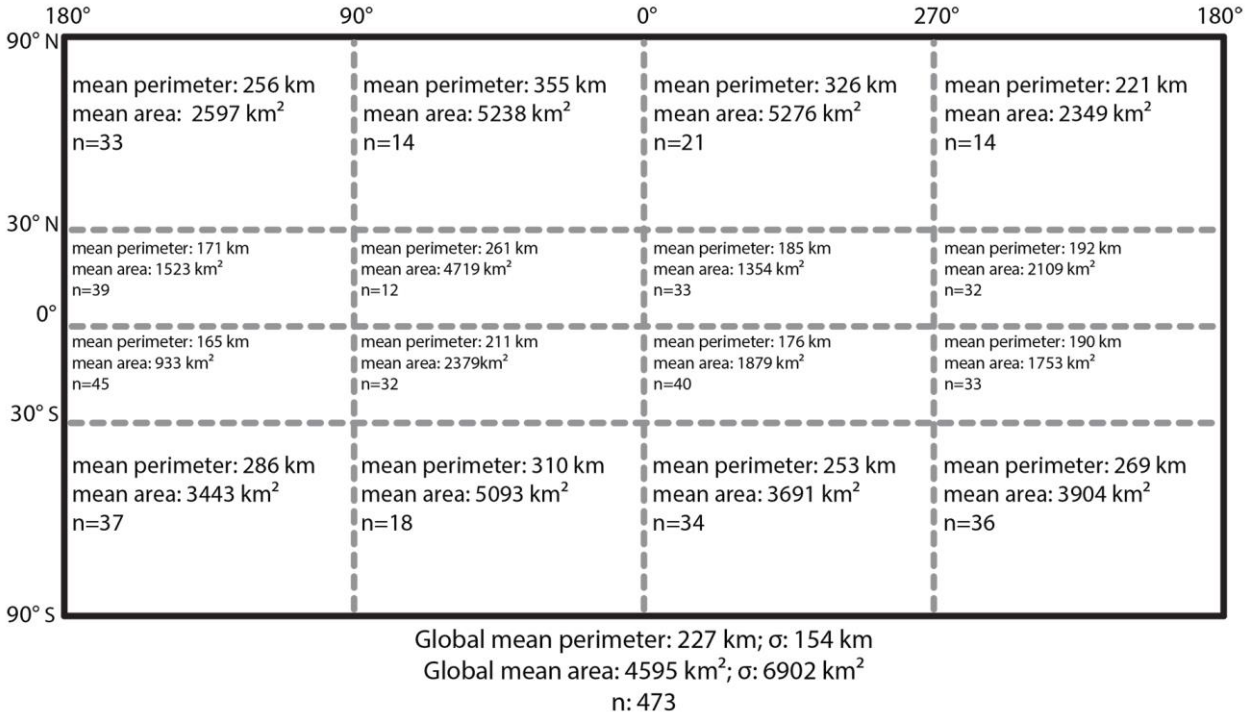

Figure 14: Patera size statistics by sector. Longitude is measured in °W.

Patera separation distances were also evaluated with the *G* function, and they plot within the predicted region, indicating there is no significant clustering. We also looked at conditional marked moments for patera perimeters and areas. Paterae with close neighbors (up to 1000 km apart) have smaller perimeters than the global average, but larger variances than we would

expect, especially with paterae 500 km apart or closer (Fig. 16). In higher latitudes, paterae tend to be larger in area, but spaced farther apart.

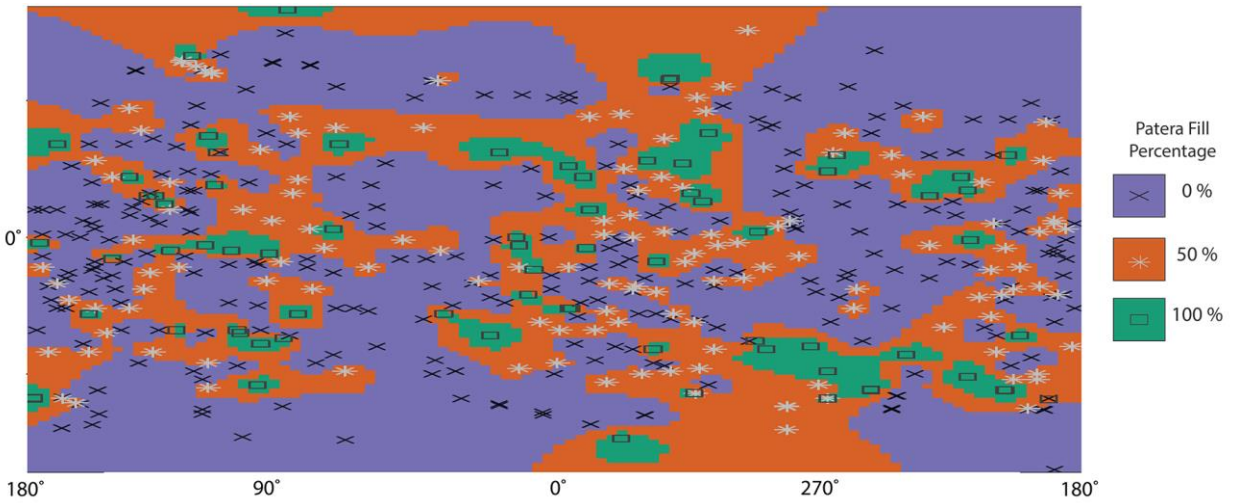

Figure 15: Smoothed view of percent fill of patera floors by location. The symbols x, ∗, and □ represent the locations of paterae with 0, 50, and 100% floor coverage, respectively.

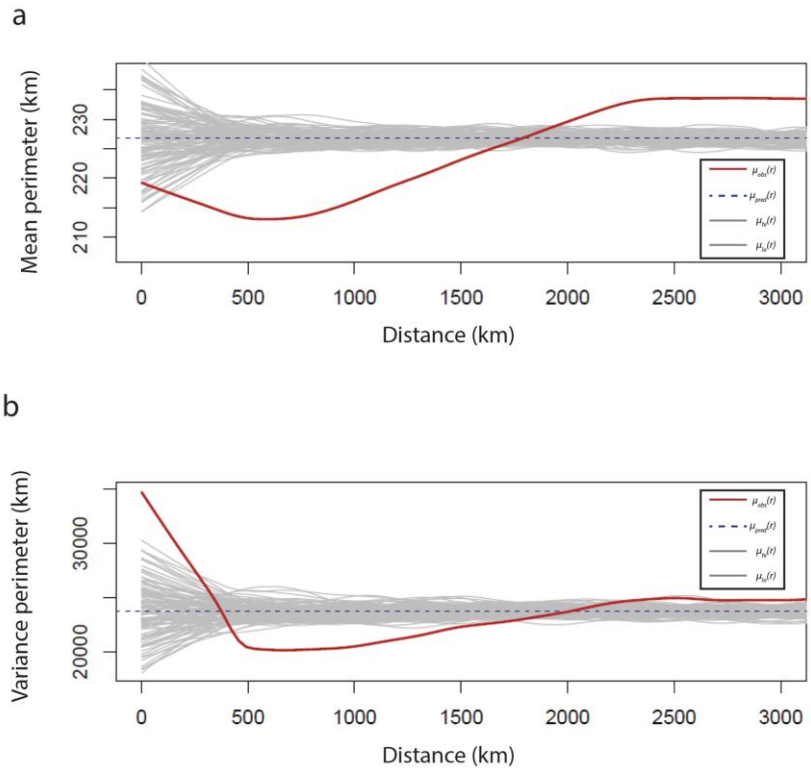

Figure 16: Conditional marked moments of patera perimeters. (a) shows the conditional mean, with global average and its bounds indicated by the dashed blue line and the grey band, respectively. The red line indicates the values for the patera perimeters in this study. (b) shows the conditional variance, with global average and its bounds indicated by the dashed blue line and the grey band, respectively. The red line indicates the values for the patera perimeters in this study.

We used pairwise Wilcoxon tests (Lowry, 2015) to look for any patterns between patera size and amount of floor coverage. Paterae that exhibit 100% floor coverage are significantly smaller in size, while paterae with floors that are either 50% or 0% covered have larger areas (Table 1). Whether this is a result of smaller paterae being easier to fill with less lava, or an indication that areas with smaller paterae are more active, is not clear at this point.

Table 1. Statistics for Patera Fill Percentage Compared with Patera Size.

		Patera Perimeter					
Fill %	Mean	Std. Dev.	Min	Q1	Median	Q3	Max
0	229.90	147.40	30.00	130.00	188.00	290.00	962.00
50	250.60	176.40	57.00	141.50	209.00	297.50	1349.00
100	171.70	119.30	25.00	95.00	151.90	218.00	705.00
		Patera Area					
Fill %	Mean	Std. Dev.	Min	Q1	Median	Q3	Max
0	4604.00	6392.90	66.68	1038.00	2408.00	5276.00	48660.00
50	5521.00	8565.80	216.70	1136.00	2621.00	5770.00	54260.00
100	2847.00	4604.00	45.08	568.50	1512.00	3127.00	33600.00

Patera Edge Lineations and Mountains.

We tested the relationships between the locations of straight patera margins and mountains with three different tests—the Equality Function, an independence test, and a random labeling test (Fig. 17). Fig. 17a shows the results of the equality function analysis. A value of 1 suggests there is no relationship between the location and type of feature. The values of the equality function are greater than 1, so statistically, features closer to each other tend to be of similar types. In other words, mountains are generally closer to each other than to straight patera margins. The same is true for straight patera edges, but this data may also be biased by the fact that many paterae have more than one straight edge to their margins. The independence test

looked at whether processes determining the locations of mountains and straight patera edges were similar or not (Fig. 17b). Since the mountain and patera edge locations, paired and plugged into the independence function, plot within the predicted range, we can assume that the null hypothesis of independence in what determines the locations of mountains and straight patera margins is valid. However, it is likely that different, yet still related, geological processes may be governing how and where these features form and their relationships to one another. The random labeling test yielded a similar result to that from the equality function (Fig. 17c).

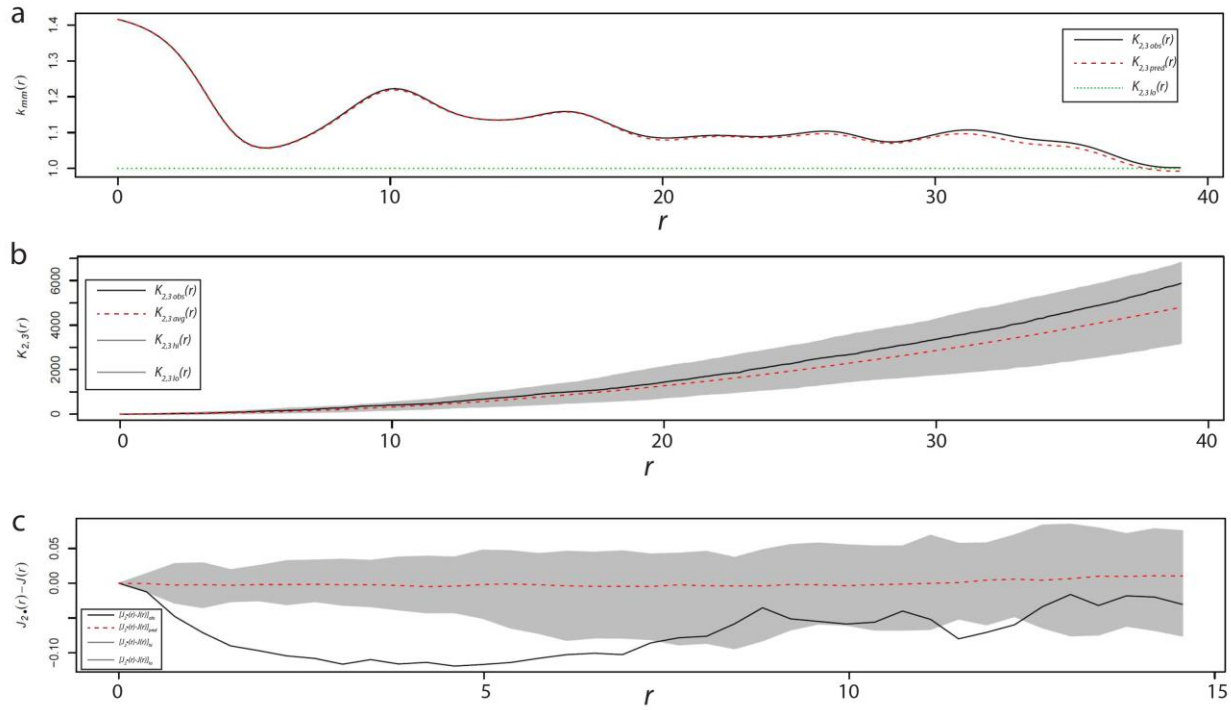

Figure 17: Relationships between mountains and patera edge lineations as revealed by (a) equality function, (b) independence test, and (c) random labelling test. Predicted average values are shown as the red dashed line and predicted bounds are represented by gray bands. Black lines indicate results from this study.

It appears that observed locations of mountains and patera edge lineations are significantly different than they would be from random assignment individually and that features close to each other tend to be of the same type. Therefore, paterae with straight edges are often closer to other paterae with straight edges, rather than to mountains. This may be due to the nature of having many more paterae than mountains on Io's surface. It seems that mountains and

paterae may be related in some cases, but we cannot conclude that mountains and paterae that appear structurally controlled will always be found in close association. There may be processes independent of mountains causing paterae to collapse along straight, sharp margins. For a better understanding of mountain-patera interaction, we wanted to get a closer look at processes driving the formation of these two features.

4. Structural Mapping

Methods

High-resolution images from the Galileo spacecraft were used to identify and interpret structures and to construct structural maps for 4 regions: Hi'iaka Montes, Shamshu Mons, Tohil Mons, and Zal Montes. These locations were selected based on the resolution of the images, the tectonic complexity, and the potential for insight into crustal deformation patterns and stress input. This work uses similar conventions to, and builds upon, geomorphic mapping by Bunte et al. (2008), Bunte et al. (2010), and Williams et al. (2004). The base images of the maps were projected orthographically to eliminate distortions using both ArcGIS and the USGS Map Projection on the Web (POW) (Hare et al., 2013). We then identified important tectonic or topographic features seen in these images and classified them as reverse faults, normal faults, grabens, strike-slip faults, mass wasting or landslide scarps, and erosional scarps. Our interpretations of the types of structural features were based on shadow observations, sense of displacement of features, scarp shape and morphology, and terrestrial tectonic analogs. Then, cross sections were generated for each area with as little vertical exaggeration as possible while preserving sufficient topographic detail. The cross sections consider the lithospheric thickness, or rather, the thickness of the uppermost brittle layer of Io, to be about 30 km based on previous studies (Keszthelyi and McEwen, 1997; Jaeger et al., 2003, Leone et al., 2011; Jozwiak, 2014).

Results

Structure of Hi'iaka Montes.

The Hi'iaka region displays the results of many of the important tectonic processes shaping Io's crust (Fig. 18). High-angle reverse faults on the western and eastern sides of the Hi'iaka Montes complex bound a large crustal block containing the two mountains. Specifically, this type of block may be similar to those bounded by high-angle reverse faults that cut the deep basement observed in Wyoming's Laramide structures (Dickinson and Snyder, 1978), indicating the possibility of a thick-skinned compressional tectonic regime on Io. The sub-parallel features on the top of the Hi'iaka plateaus are tens of meters deep and tens of meters across (Bunte et al., 2010) and were likely created in response to the uplift of the mountains as grabens formed from extension above the neutral surface of the fold. Alternatively, it is possible that these features are small-wavelength folds with orientations reflecting the orientation of σ_1, although the rigid properties of the upper crust may prohibit formation of such small-scale folds.

Shortening of the crust in this area oblique to the bounding reverse faults has produced a dextral strike-slip fault running between the two mountains, breaking apart the larger crustal block. This is based on interpretations made by Jaeger et al. (2003) and Bunte et al. (2010) and by further identification of features associated with a strike-slip system in this study. The northern arm of North Hi'iaka Mons has accommodated the oblique strike-slip motion through restraining bends, which have built up the ridges that make up the highest elevations in the area, up to 11 km (Schenk et al., 2001). The transpressional features in this area are similar to the transpressional ridges running through Damascus and Palmyra, Syria formed along a restraining bend in the Dead Sea Fault (Mann, 2007), and the way transpression is accommodated mostly by vertical displacement is similar to structures adjacent to the San Andreas Fault zone near San

Bernardino, California (Spotila et al., 1998). The restraining bends on North Hi'iaka Mons have also bent the localized extensional features on the top of the plateau, suggesting that the grabens formed either just before or simultaneously with strike-slip movement.

On the southern edge of South Hi'iaka Mons, a very different response seems to be occurring than is happening in the north. Instead of transpressional features building up tall peaks, normal faults and extensional collapse have shaped the south edge of South Hi'iaka Mons. A large valley separates the northern, cohesive part of the mountain from the collapsing side on its southern end. Extensional faults and gravitational failures parallel to the southern arm of South Hi'iaka Mons indicate that the main processes in this area are rifting and collapse. The apparent difference between the northern edge of North Hi'iaka Mons and the southern side of South Hi'iaka Mons may be due to crustal anisotropy or differential rate of movement along the faults in the area. South Hi'iaka Mons has possibly not met resistance in the crust either by composition or buried structures. It also could be moving more rapidly south than other parts of the complex along the main strike-slip fault running through the middle of the larger block. Younger volcanic layers cover many of the important structures or crustal block boundaries in the region surrounding the Hi'iaka mountains (Fig. 18b), due to Io's constant and rapid resurfacing. Therefore, it is not entirely clear how the Hi'iaka block is interacting with other large blocks around it or the precise locations of some faults. We can only draw conclusions from those structures and related features that are currently visible.

In addition to producing transpressional features, this regime has also opened transtensional basins on the eastern side of North Hi'iaka Mons and the western side of South Hi'iaka Mons. An active patera has formed in the northeastern basin, possibly facilitated by the rifting that occurred as a result of strike-slip movement on the bounding faults.

In the southwestern basin, there is a small peak, West Hi'iaka Mons (Fig. 18). It may have separated from southern Hi'iaka Montes in a similar fashion to Madagascar as it broke off from the northward-moving Indian plate and was isolated in the ocean basin just east of Africa. This small "island" could have rifted from either the southern margin of North Hi'iaka Mons or the northern side of the arm of South Hi'iaka Mons and was left as South Hi'iaka Mons continued to move away from North Hi'iaka Mons. The surrounding plains appear smooth, indicative of deposition or infilling of volcanic materials, which again could have been facilitated by subsurface structures or the opening of the basin and thinning of the crust. Additionally, it appears that a normal fault exists on the southern side of the "island", further emphasizing an extensional input to its tectonic history.

In the northeastern basin, minor shortening apparently occurred at one time, as indicated by long arcuate scarps that we relate to reverse faults in Fig. 18. They must have formed after or during strike-slip motion because they are overprinted on the basin-filling deposits.

It is unclear whether there is a significant relationship between South Hi'iaka Mons and Shamshu Mons, which lies just southeast of the southeastern corner of South Hi'iaka Mons and is shown in detail in Fig. 19. Although the southern arm of South Hi'iaka Mons is parallel to the long axis of Shamshu, they are separated by ~70 km and the features on each mountain do not seem to indicate that they are in tectonic "communication." The plain between the two may contain a buried major reverse fault, separating the Hi'iaka block and the Shamshu block and keeping the two mountains from interacting directly with one another. Consequently, it is unlikely that the Hi'iaka Montes complex is in any way directly causing the uplift of Shamshu Mons.

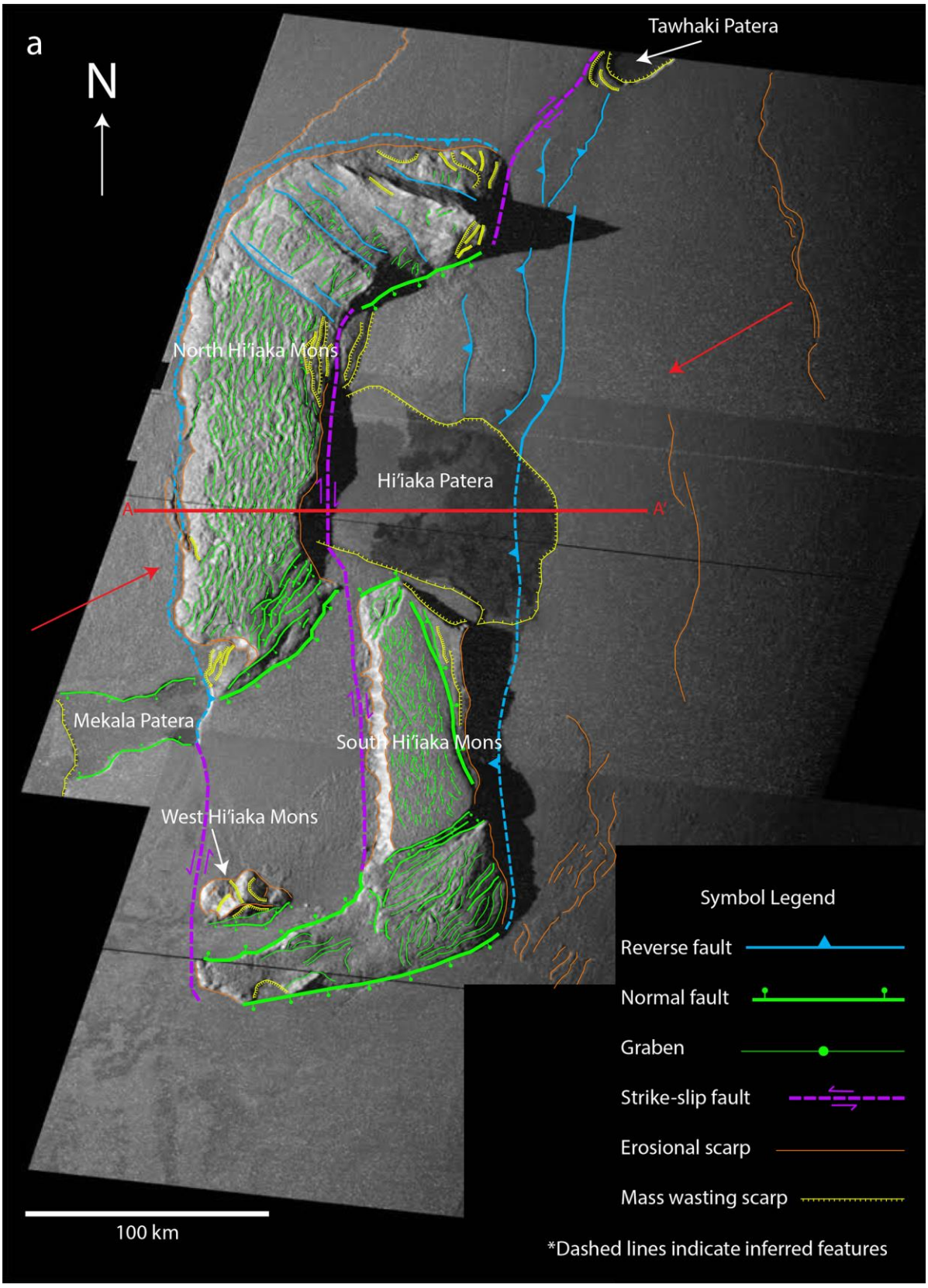
a
N
Tawhaki Patera
North Hi'iaka Mons
Hi'iaka Patera
A
A'
Mekala Patera
South Hi'iaka Mons
West Hi'iaka Mons
100 km
Symbol Legend
Reverse fault
Normal fault
Graben
Strike-slip fault
Erosional scarp
Mass wasting scarp
*Dashed lines indicate inferred features

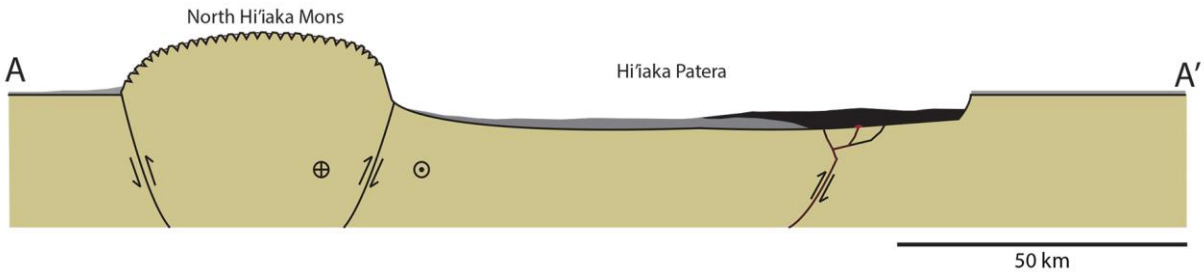

Figure 18: Hi'iaka Region (3.5°S, 79.5°W). (a) Reprojected Galileo image (~250 m/pixel) of the Hi'iaka Montes complex with structural interpretations. Image was obtained during the I25 flyby on November 26, 1999. Illumination from the left (west). The red arrows indicate proposed orientations of principal horizontal stresses, σ_1 (previous page). (b) Cross section from A to A' (a) across North Hi'iaka Mons and Hi'iaka Patera. Fresher eruptions on the patera floor are black, with older flows indicated by gray. Major mountain bounding faults are interpreted to have oblique slip with strike-slip and reverse movement. The vertical axis is unscaled but vertical exaggeration is about 2x.

In short, the tectonic history of the Hi'iaka region appears to be to be governed by largely buried, pre-existing faults in the deeper crust that were reactivated obliquely by continued shortening of the crust. It seems most likely that North and South Hi'iaka Mons are part of a large, coherent crustal block that has been uplifted and modified by shortening of the crust, with maximum stresses at oblique angles to faults previously formed and then buried by the volcanic deposits. Loading by volcanics and subsequent horizontal shortening of the crust was a hypothesis first presented by Schenk and Bulmer (1998) in their discussion of the Euboea Montes area. The idea of strike-slip modification in the Hi'iaka area was discussed by Bunte et al. (2010) in their geomorphic mapping. We build upon both of these concepts by combining them—shortening of the crust with maximum stress oblique to pre-existing basement faults has produced strike-slip motion and its associated features in this area. We have identified important features in this area in enough detail to suggest both an origin and a context for them.

Structure of Shamshu Mons and Patera.

The Shamshu region is located just southeast of the Hi'iaka region. Shamshu Mons is about 180 km long and stands 3 km above the surrounding smooth plains. We have interpreted

the arcuate features on its northwest and southeast sides as reverse faults. Shamshu is steeper on the northwest side, and its southeast side has a gentler slope, due to the asymmetrical nature of the underlying fold and associated thrust faults or from differential movement along its faults. The southeast flank is also marked by gravitational slumps whose headwalls are approximately parallel to the crest of the massif. The NE-trending valley that runs through Shamshu Mons parallel to its long axis is likely a graben formed from localized extension above the neutral surface at the axis of the asymmetric fold. Additionally, the floor of the graben in Shamshu Mons is smooth and at the same elevation as the surrounding plains, suggesting that it may have been resurfaced recently; dark flow lobes extend from the rim of Perun Patera northward and fill the graben. Shamshu Mons gives way to a plateau on its southeastern side. A fault appears to terminate the plateau and separate it from the smooth plains containing Shamshu Patera. Its arcuate shape and similarity to the margins of Shamshu suggest that it is a late reverse fault that cut lava flows on the plain, and then the scarp was partially buried by more volcanism.

Shamshu Patera is likely bounded by randomly oriented collapse margins. They do not show conclusive evidence that they are tectonic in nature, given that they do not continue beyond the margins of the patera. The patera as a whole was probably larger in the past than it is currently. The arcuate features just northwest of "South Shamshu Mons" (Bunte et al., 2010), the mountain in the southeast corner of the image (Fig. 19), may be remnants of the patera's edges at one point in its history. They could have become less defined by sapping or erosion, collapse and mass wasting, or by infill of the patera when it may have been more active and before activity shifted to the east.

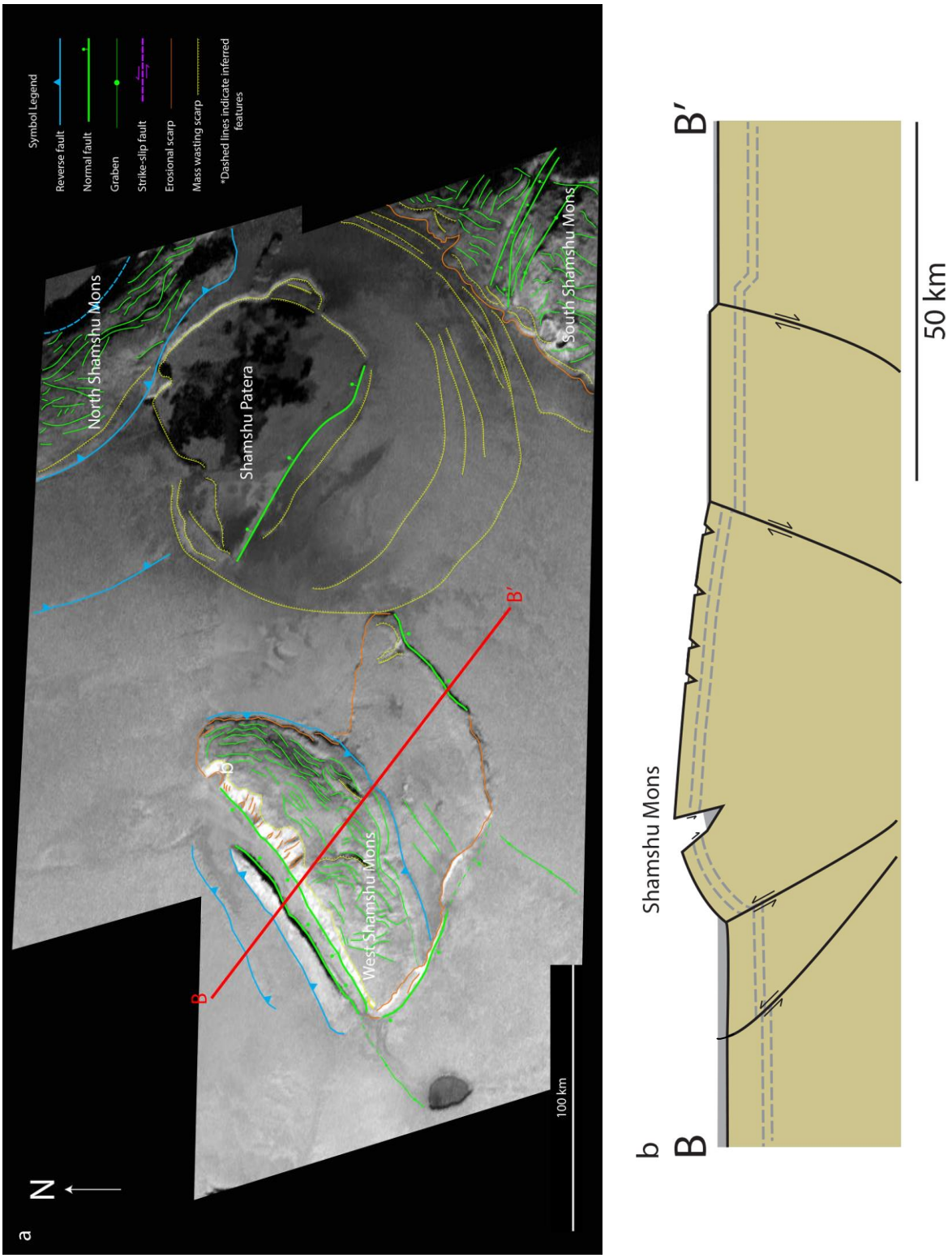

Figure 19: Shamshu Mons and Patera (9.0°S, 68.0°W). (a) Reprojected mosaic of Galileo images (~345 m/pixel) of the Shamshu region and structural interpretations. Image was obtained during the I27 flyby on February 22, 2000. The red arrows indicate proposed orientations of principal horizontal stresses, σ_1 (left). (b) Cross section from B to B'(right) as indicated on (a). The dashed gray line represents the behavior of crustal layers in the subsurface. The vertical axis is unscaled but vertical exaggeration is about 2x.

We interpret the faults bounding the mountain to the northeast, "North Shamshu Mons" (Bunte et al., 2010), as reverse faults. Shamshu Patera has incised the side of North Shamshu Mons adjacent to it, suggesting it is younger than the mountain. The top surface of North Shamshu Mons is lineated, probably fractured due to localized extension from folding and uplift. South Shamshu Mons, in the southeast corner of the image, is also heavily lineated. It too could be bounded by thrust faults, or by a normal fault on the side facing Shamshu Mons, but these may have lost surface expression due to fracturing, mass wasting, or the previous boundaries of Shamshu Patera. Without full context from above, we cannot tell the orientations of the long axes of North and South Shamshu Mons and therefore cannot say whether they could have previously combined with Shamshu Mons to make one large mountain as suggested by Bunte et al. (2010), or if they were formed independently in separate fault-bounded blocks under similar or multiple stress regimes. From what the images reveal, the long axis of North Shamshu Mons is perpendicular to Shamshu Mons and therefore may not have been formed under the same stress regime. The extensional fault on the southeast plateau adjacent to Shamshu Mons and the smooth plains between Shamshu Mons and South Shamshu Mons may indicate rifting and subsequent volcanism has occurred between them. Unfortunately, subsurface structures are covered by multiple layers of volcanic material, obscuring a more complete interpretation of the tectonic history of the Shamshu region.

Structure of Tohil Mons.

The Tohil region is a site of active volcanic, tectonic, and degradational processes. Tohil Mons, the main feature in the image (Fig. 20), is 350 km long and about 5.4 km high (Schenk et al., 2001). It likely sits on its own fault-bounded crustal block, although the complete extent of the block is unclear, as the plains surrounding the mountain complex have been resurfaced by

volcanism. The mountain seems to be bounded by reverse faults, with a strike-slip fault running down its long axis (Fig. 20).

Like Hi'iaka, Tohil Mons was probably built and modified by shortening and strike-slip motion in a large, crustal block. Maximum horizontal stress was likely oblique to pre-existing NW-trending basement faults and block-bounding faults, which induced strike-slip movement on what was probably a near-vertical fault. Graben-like features on the elongated plateaus of Tohil may be like those on the plateaus of the Hi'iaka mountains, formed by extension above a neutral surface in a large fold or through gravitational slip. This may also be how the extensional faults and grabens formed on the failing northeast lobe of Tohil Mons. The margins of Tohil have been eroded, possibly through SO_2 sapping, far more than those at Hi'iaka seem to have been. The major faults bounding the Tohil block have likely been buried or obscured by erosional scarps, landslide material, or volcanic cover.

Radegast Patera seems to have formed in a transtensional basin that opened as a result of dextral motion along the NW-trending strike-slip fault, similar to the way in which the basin formed that contains Hi'iaka Patera. The sense of downward motion along the oblique-slip fault seems to be to the northwest of the landslide "crater" and to the southeast of the landslide "crater". Instead of being attributed to a multiple fault system, this difference in motion could result from a difference in topographic level between the two halves, in which the northeast side is higher. The northeast portion seems to be experiencing greater gravitational degradation by landsliding than anywhere else along the fault, further supporting the idea that this part of the mountain is higher or steeper than other locations.

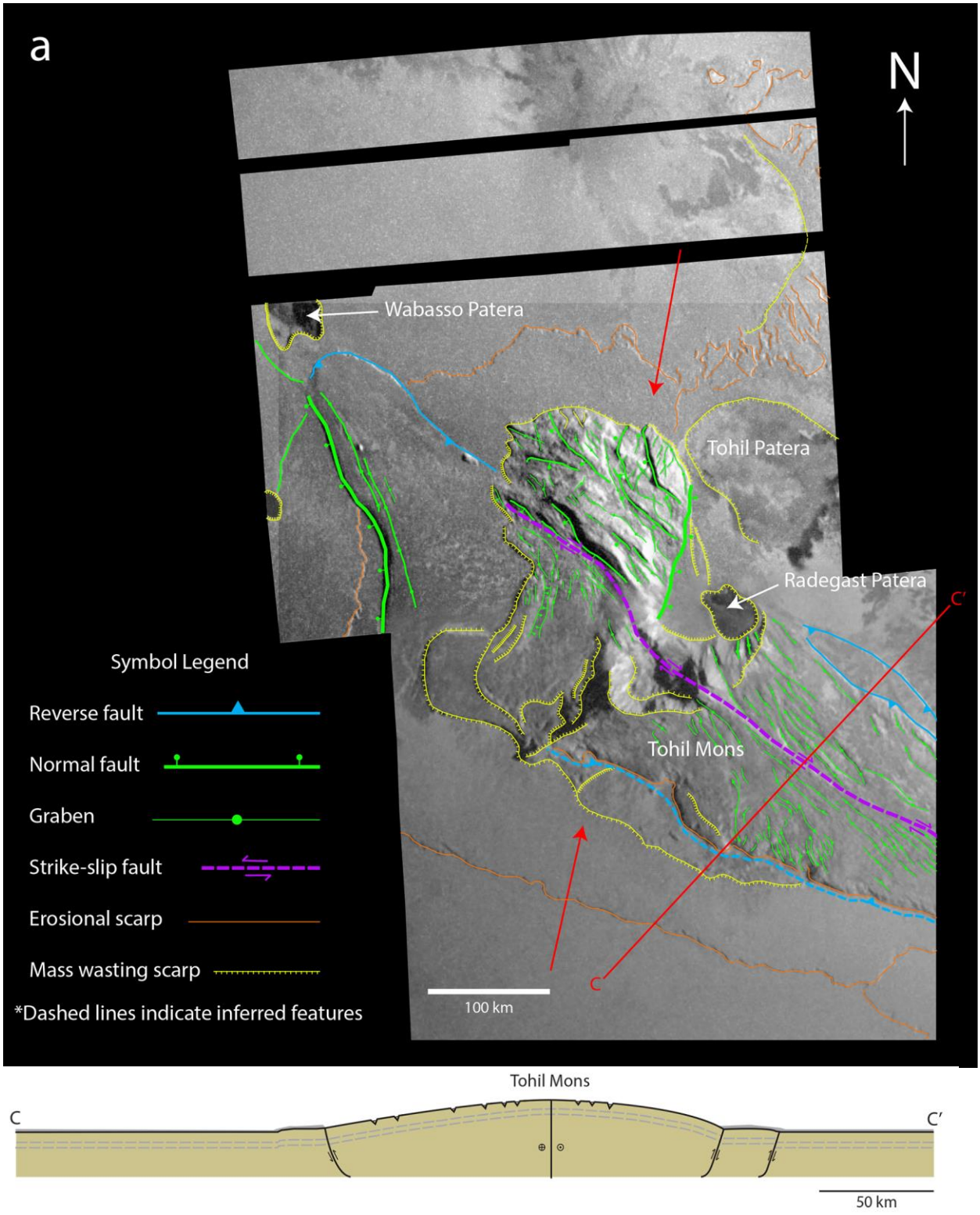

Figure 20: Tohil Region (28°S, 161°W). (a) Galileo image mosaic (~327 m/pixel) of Tohil Mons, overlain by structural interpretations. Images were obtained in October 2001. Illumination from the upper right (northeast). The red arrows indicate proposed orientations of principal horizontal stresses, σ_1 (above). (b) Cross section from C to C' (below) as indicated in (a) across Tohil Mons. No vertical axis is specified but vertical exaggeration is about 5x.

The central "crater" of Tohil Mons is the result of a large slump, whose material has both collected in the floor and been consumed by the formation of Radegast Patera. Further landslides extend to the northeast, probably onto the floor of Tohil Patera. On the western side of the depression, large amounts of slumped material have created large lobes and a ridge-forming scarp extending from the scarp crater wall to the southwest. The west-trending ridge may be made of more resistant material or could simply be the scar from the large landslides. It is possible that the ridge is a resistant dike, as it is in line with Radegast Patera and the fissure eruptions actively occurring on the floor of Tohil Patera when the image was taken, but no other features indicate that Tohil Mons is volcanically built or fed. It seems more plausible that the summit "crater" is a result of mass wasting, since it is surrounded by slumped material.

A large-offset, steep, normal fault appears to have formed the northwest margin of Tohil, aligned with Wabasso Patera, possibly feeding magmatism to that area. It is unclear how extension is consistent with the other observed structures in the region if there is one major stress field unless this fault marks an extensional basin within the northern block that is not visible in this image. Therefore, multiple stress fields may have been in effect at different times, where extension was preceded by shortening and dextral motion within the block. The block may also be responding to deeper, pre-existing structures or crustal differences that are not visible at the surface. This could mean that extension could be so localized that it is only happening in that area.

Structure of Zal Montes.

Even visually, the two mountains of the Zal region are very different from each other (Fig. 21). North Zal Mons is a nearly flat, smooth plateau, with straight margins that, although scalloped by erosion, are still quite linear. The plateau is ~250 km long and stands about ~2 km

above the surrounding plains (Schenk et al., 2001). South Zal Mons, however, has more arcuate boundaries and a lineated, rugged top surface with a narrow ridge crest towards its southern end. It is 7.4 km in height (Schenk et al., 2001). In addition to morphological differences, the long axes of these two mountains are roughly perpendicular to one another. These contrasting features and orientations argue that each part formed at different times under different stress regimes or that they formed independently of one another. It is unclear whether the mountains exist on one large crustal block or two separate blocks. The evidence for either scenario is buried below the surface.

North Zal Mons does not seem to have experienced the same styles of crustal deformation as those experienced at South Zal Mons or, for that matter, the other mountains described above. North Zal Mons has been fractured on its southern side, but this is likely due to extension and gravitational slumping in concert with larger-scale extensional faults that bound its southern side. In fact, we have interpreted all of the major boundaries of North Zal Mons as normal faults, due to both their straight natures and to the fact that we see no evidence of crustal shortening on the plateau. There may be later minor reverse faulting south of North Zal Mons as evidenced by faint, arcuate features in the plain to the south, but these do not seem to interact with or cause any deformation to North Zal Mons itself. North Zal Mons may be a remnant of older, more resistant crust that has been separated from its surroundings, not by uplift, but rather by the plains around it sliding away as a result of extension. This seems the most likely possibility given the morphology and geometry of North Zal Mons and the tectonically-formed lineations on and around it.

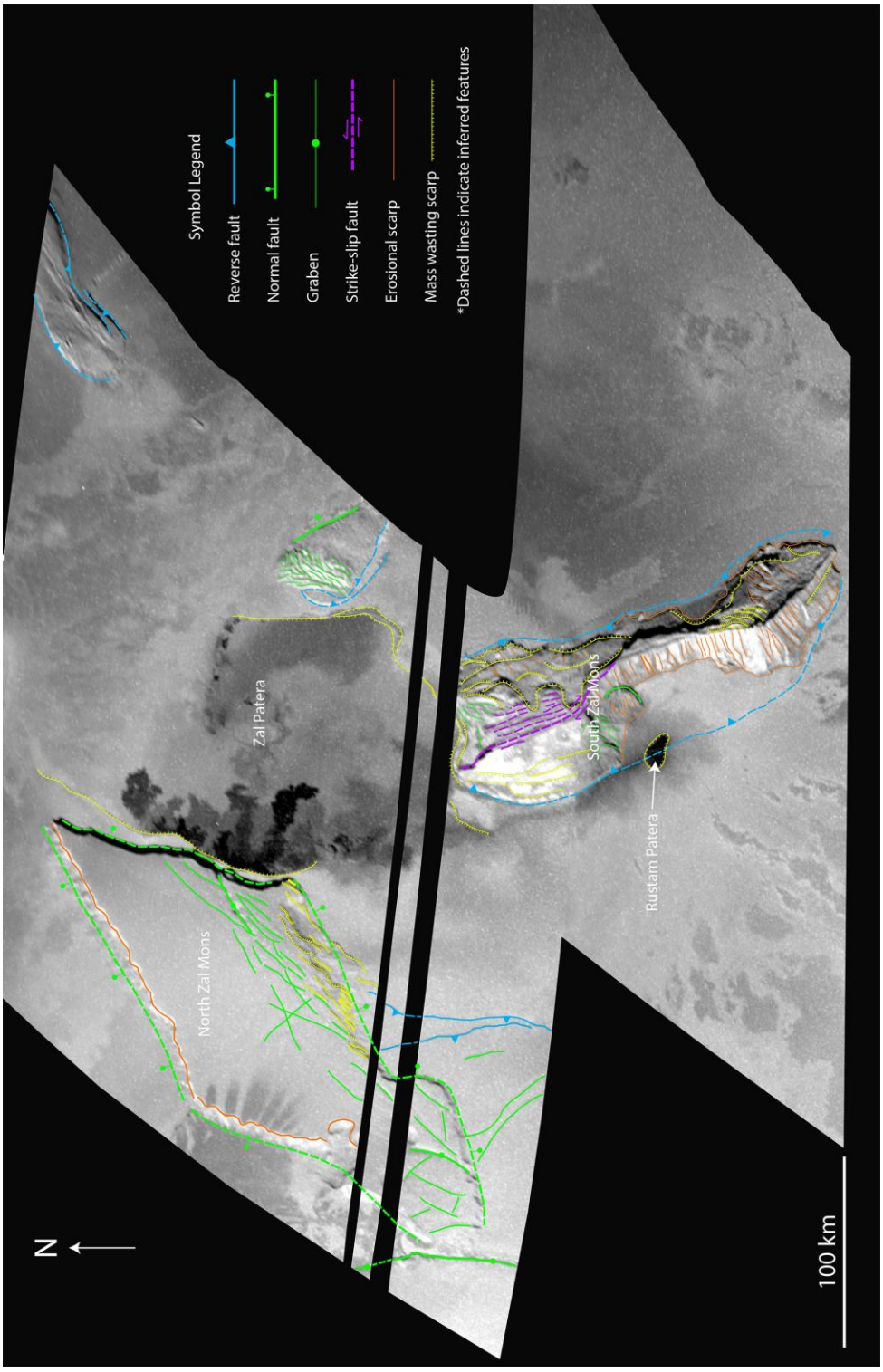

Figure 21: Zal Region (33.7°N, 81.9°W). Reprojected Galileo images (~260 m/pixel) of the Zal Montes complex, with structural interpretations. Images were obtained November 26, 1999 and February 22, 2000. Illumination from the left (west).

South Zal Mons, however, shows evidence of horizontal shortening as it has built up steep, tall sides along fairly arcuate boundaries. We interpret these as high-angle reverse faults such as those seen elsewhere on Io. The basin on the west of South Zal Mons that causes its asymmetrical shape may not have always existed. Rather, it is possible that the ridge on the north of South Zal Mons is a right-lateral strike slip fault that has moved the two halves of the mountain apart to form the basin. As this space opened, blocks on South Zal Mons' steep western side slumped towards the west. The strike-slip motion that has moved the eastern half of South Zal Mons to the south may be the cause of the rather abrupt western face adjacent to the transtensional basin.

The volcanic activity in the area is structurally controlled. Fresh flows on the floor of Zal Patera line up with the bounding normal faults of North Zal Mons. Additionally, Rustam Patera lies along a block-bounding oblique reverse fault that may have opened the basin it currently resides in on the western side of South Zal Mons. This further shows how fractures and faults in Io's crust serve as magma conduits.

Although Bunte et al. (2008) proposed that the two mountains of Zal were once joined together and subsequently separated through strike-slip motion and rifting, we do not see geomorphic or tectonic evidence that conclusively supports the hypothesis that they were once a single structure. There appears to have been little to no crustal shortening to the north, given the margins of North Zal Mons. However, South Zal Mons is an entirely different and complex structure that was involved in significant crustal shortening. On the undistorted, reprojected images used in this study, the different parts of the block that were joined together by Bunte et al. (2008) no longer appear to fit. Instead, we propose that North and South Zal Montes never were one mountain but rather that they formed independently. They may be separated by block-

bounding faults buried beneath Zal Patera. Nonetheless, this area is challenging to understand; the visible structures can be interpreted in multiple ways, and much of the possibly telling structural features are buried under smooth volcanic plains. We present an alternative hypothesis, yet recognize that there are strengths and weaknesses to any model since data for the Zal region is limited.

5. Discussion

We propose that Io's mountains result from multiple stress inputs through global and local-scale processes. Over time, relatively uniform resurfacing by volcanism could generate compressive vertical stress on the crust sufficient to produce local uplift of large, coherent crustal blocks bounded by deep-rooted, high-angle reverse faults, as proposed by Schenk and Bulmer (1998). These may be similar to basement-cored, thick-skinned contractional features found on Earth, such as the Laramide-style mountains of Wyoming, USA (Fig. 22; Wise, 1963). Although resurfacing is likely the main player in global crustal stress, it is also possible that variable stresses produced by tidal massaging are a factor. The preferred orientations of structural lineations observed in this study at 45° and 135° show that horizontal shortening of the crust is occurring in addition to vertical stresses being imposed by global loading and contraction. Lateral compression of Io's crust may be a result of diurnal tidal stress fields. The fact that the greatest concentrations of structure orientations are 90° apart from each other could indicate one maximum stress direction, σ_1, and one direction of least stress, σ_3. However, the two preferred orientations could also indicate two different global stress fields occurring at different times, with both orientations indicating a different σ_1. Stresses from tidal forces vary diurnally as well as on larger timescales due to slightly non-synchronous rotation of Io. Additionally, stresses vary by location on its surface. In equatorial regions, predicted maximum stresses are virtually equal

in both the north-south and east-west directions and these stresses become increasingly oblique towards the poles. Stresses also vary depending on longitude as the tidal bulge both stretches toward Jupiter and relaxes throughout an Io day while lagging slightly behind the rotation rate of the moon as a whole (Bart et al., 2004). It is very likely that the observed orientations of structural features at 45° and 135° are a product of tidal stresses—both from the constant massaging of the moon and the variation in those stresses imposed by orbital properties and by location on its surface. Although global contraction by volcanic loading is causing shortening throughout Io's crust through vertical stresses, overprinting by stresses induced by tidal forces may be governing the orientations of many structural lineations by lateral horizontal crustal shortening.

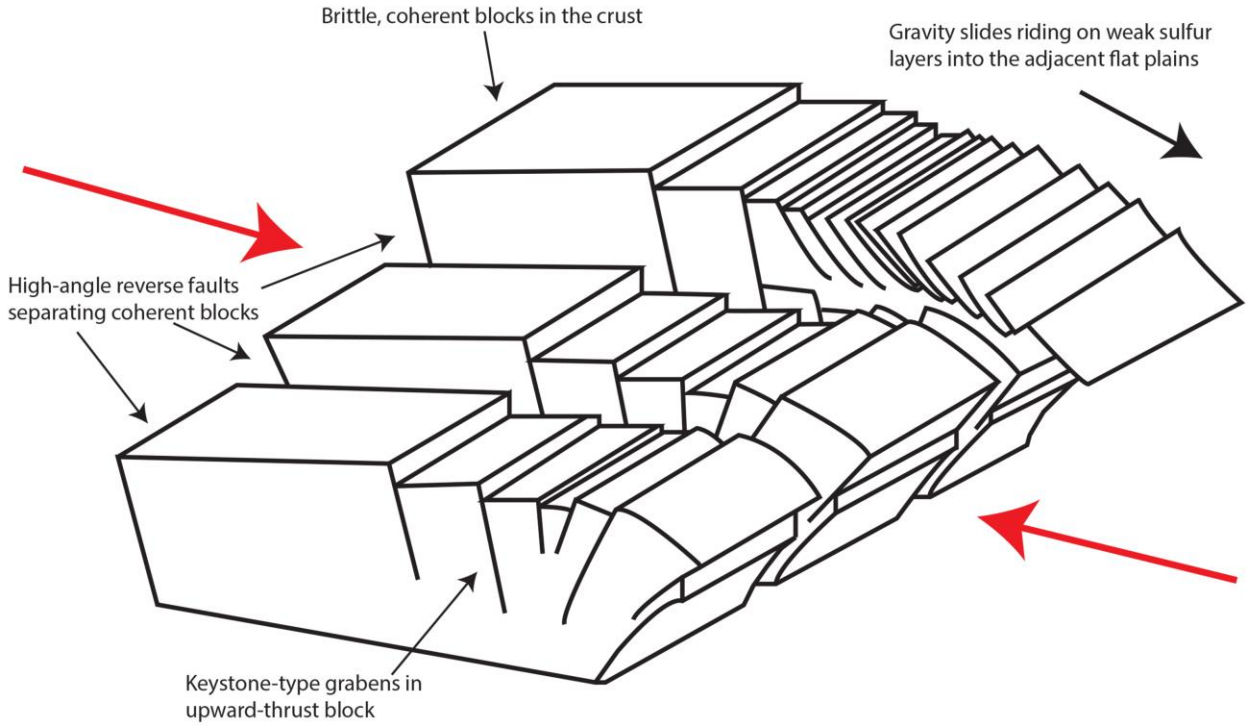

Figure 22: Generalized block diagram of the formation and evolution of many of Io's mountains, based on Laramide-style basement-cored uplifts seen throughout Wyoming. The red arrows indicate theoretical orientations of principal horizontal stresses, σ_1. Modified from Wise (1963).

While the cause of mountain formation may be more global in nature, the details of mountain formation and evolution and patera collapse are determined by pre-existing structures in the crust. Throughout geologic time and through consistent global stress by volcanic loading (Schenk and Bulmer, 1998) and tidal flexing (Bart et al., 2004), fractures and faults built up in the crust and were subsequently buried under successive episodes of volcanism. Then, as stresses continued, basement faults were reactivated, many by stresses oblique to those that originally formed the faults. This produced oblique strike-slip motion and initiated formation of transtensional and transpressional features along these faults. Transtensional basins opened to allow for thinning of the crust and possible patera formation or magma migration along structures. Crustal blocks continued to move in various directions depending on the orientations of maximum horizontal stress and orientations of basement faults. This explains the seemingly random orientations, locations, shapes, and sizes of mountains on Io. Some mountains gently arch while others are more polygonal and straight. At least a few are bounded by faults with dominantly normal offsets; others by broadly arcuate, high-angle reverse faults. Mountains on Io represent a combined effect of global and regional tectonic processes, and it is necessary to account for the input of both. Fig. 22 and Fig. 23 display some of the most important processes in building and modifying some of these mountains. All mountains, however, can claim modification by sapping of volatiles in the crust and by mass wasting and gravitational collapse of over-steepened slopes. These local-scale processes can be seen virtually everywhere a feature of topographic relief appears on Io's surface.

Deformation on Io is likely thick-skinned rather than thin-skinned because of the nature of Io's crust and structures contained within it. Since Io's crust is most likely basaltic, it is more likely to experience brittle, rather than ductile, deformation. Sulfur-rich layers interbedded within

mafic volcanics could provide zones of weakness, but overall, Io's crust is considered to be composed of basalts, or possibly ultramafics (McEwen et al., 1989; Carr et al., 1998; Geissler et al., 1999; McEwen et al. 1998; McEwen et al., 2000; Radebaugh et al. 2004). Therefore, we would expect Io's crust to be broken into large, coherent blocks with deep, high-angle reverse faults such as those in the Laramide-formed mountains of the western United States (Fig. 22; Brewer et al., 1982).

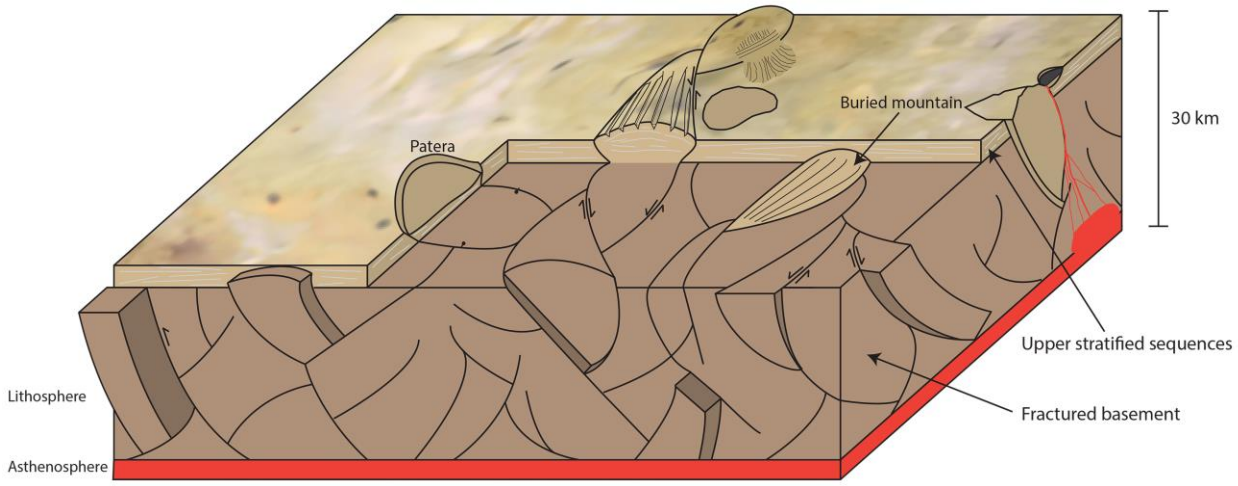

Figure 23: Generalized block diagram of the basement fault model presented in this study. From global stress inputs such as tidal forces and volcanic loading, oblique stresses to pre-existing basement faults create transtensional openings, transpressional folding, and reverse and normal faulting. Crustal blocks move in various directions depending on the direction of maximum stress and the orientations of basement faults. Paterae are able to form along structural features, such as in transtensional basins, and subsurface faults can act as magma conduits to facilitate eruptions onto patera floors.

We can assume that tidal forces and volcanic loading on the crust have been at work for millions of years, and therefore have been responsible for some or all of the deformation of Io's crust. It would follow that there would be many faults and fractures in the subsurface, obscured to our view today, but that would be continuing to affect surface topography. Stresses on the crust would exploit and reactivate these structures to continue deformation. The Laramide Orogeny and its associated thick-skinned tectonic regime resulted from shallow subduction causing stress to accumulate in the base of the crust (Brewer et al., 1982). Similar stresses may be generated on

Io, not from subduction of tectonic plates, but rather from convective upwelling of partially melted materials, from deep, internal stresses from tidal massaging, or from consistent burial and shortening of the global radius by volcanic loading. However these stresses are generated, all would result in the thick-skinned style of crustal deformation (Schenk and Bulmer, 1998; Schenk et al., 2001; Jaeger et al., 2003; Bart et al., 2004).

6. Conclusion

Io has some of the tallest and steepest mountains in the solar system and they are uniquely shaped and formed. Tectonics operating on Io, a body with a continuous source of stress and internal heat are automatically quite different from those creating Earth's mountains and volcanoes. It seems that Io's mountains form as islands amidst smooth, continually resurfacing plains, and are remnants of older, highly fractured crust uplifted and modified by both global and local tectonic processes. Although there are still fundamental questions to be answered about crustal properties and mechanics on Io, this model begins to address them. Io's crust is probably broken into relatively large blocks, bounded by reverse faults, indicating that crustal response is more brittle than ductile in nature. This supports the idea that Io's crust is mostly basaltic. However, zones of weakness that allow the crust to rupture may mark regions of sulfur concentration that have accumulated from past plume eruptions.

Movement of crustal blocks in relation to each other may be governed by zones of partial melt that are fairly shallow, or this movement may instead be governed purely by the stresses imposed on a brittle crust by tidal massaging and volcanic loading. We do not know the exact nature of subsurface structures, but based on features visible at the surface, it seems that Io's crust is very much fractured and faulted. The morphology of and statistical results describing topographic features suggest that the mountains on Io have been formed under multiple stress

regimes. We can assume that stress regimes have been varying throughout Io's existence and this has left the crust broken up in many orientations. To more fully understand Io's complex tectonic systems would require detailed interpretation of both large and small-scale faults, fractures, and other structural features across Io, though very few regions have been imaged at high enough resolution. While low image resolution obscures some of these features, it is Io's intense resurfacing (~ 1 cm/year) (Johnson et al., 1979) that covers many telling structural features.

Io's lithospheric characteristics, such as its thickness, thermal gradient, depth of recycling, and density differences, are at best speculative currently. Therefore, it is unclear whether delamination of the lithosphere and its associated vertical stresses would be a factor in the creation of Io's mountains. It can still be concluded that tidal stresses and global contraction by loading have played a role in deformation of Io's crust into coherent crustal blocks. We can also say that the lithosphere is sufficiently thick to support mountains up to 17-18 km in elevation (Schenk et al., 2001), given the unique compositional and buoyancy constraints of Io's lithosphere.

A greater understanding of Ionian tectonics and lithospheric properties is key to our knowledge of the workings of tectonics on other bodies in the solar system. A world of extremes, Io provides insight into tectonic features on other planets and moons since it has so many available for study. The way volcanic and tectonic processes interact on Io serves as a starting point for other tidally heated bodies of the outer solar system. While many of the icy moons of the outer solar system are receiving current attention for their possibilities of harboring life, Io also has a wealth of information to offer as one of the extreme bodies of the solar system and as a potential model for early Earth conditions when it was still hot and before the onset of plate tectonics.

References

Anderson, J.D., Sjogren, W.L., and Schubert, G. (1996). Galileo gravity results and the internal structure of Io. *Science, 272,* 709-712.

Bart, G.D., Turtle, E.P., Jaeger, W.L., Keszthelyi, L.P., and Greenberg, R. (2004). Ridges and tidal stress on Io. *Icarus, 169,* 111-126.

Barth, B. and Radebaugh, J. (2010). Distribution and comparison of Io's paterae: Effective diameters and active volcanism. *41st Lunar and Planetary Science Conference,* Abstract #2666.

Blaney, D.L., Johnson, T.V., Matson, D.L., and Veeder, G.J. (1995). Volcanic eruptions on Io: Heat flow, resurfacing, and lava composition. *Icarus, 113,* 220-225.

Brewer, J.A., Allmendinger, R.W., Brown, L.D., Oliver, J.E., and Kaufman, S. (1982). COCORP profiling across the Rocky Mountain Front in southern Wyoming, part 1: Laramide structure. *Geological Society of America Bulletin, 93,* 1242-1252.

Bunte, M.K., Williams, D.A., and Greeley, R. (2008). Geologic mapping of the Zal region of Io. *Icarus, 197*, 354-367.

Bunte, M.K., Williams, D.A., Greeley, R., and Jaeger, W.L. (2010). Geologic mapping of the Hi'iaka and Shamshu regions of Io. *Icarus, 207*, 868-886.

Carr, M.H., McEwen, A.S., Howard, K.A., Chuang, F.C., Thomas, P., Schuster, P., Oberst, J., Neukum, G., Schubert, G., and the Galileo Imaging Team. (1998). Mountains and calderas on Io: Possible implications for lithosphere structure and magma generation. *Icarus, 135*, p 146-165.

Cruikshank, D.P. and Nelson, R.M. (2007). A history of the exploration of Io. *Io After Galileo*, Springer, Chichester, UK, 5-33.

Davies, A. (2001). Volcanism on Io: The view from Galileo. *Astronomy and Geophysics, 42* (*2),* 2.10-2.15.

Dickinson, W.R. and Snyder, W.S. (1978). Plate tectonics of the Laramide orogeny. *GSA Memoirs*, *151,* 355.366.

Funk, C. (2011). Intensity analysis of spatial point patterns. *Online*. http://www.geog.ucsb.edu/~chris/Lecture5_210C_Spring2011_PointPatternInteractions.pdf. Accessed 27 Jan 2016.

Geissler, P.E., McEwen, A.S., Keszthelyi, L., Lopes-Gautier, R., Granahan, J., and Simonelli, D.P. (1999). Global color variations on Io. *Icarus, 140,* 265-282.

Hamilton, C.W., Beggan, C.D., Still, S., Beuthe, M., Lopes, R.M.C., Williams, D.A., Radebaugh, J., and Wright, W. (2013). Spatial distribution of volcanoes on Io: Implications for tidal heating and magma ascent. *Earth and Planetary Sciences Letters*, *301,* 272-286.

Hare, T., Akins, S., Sucharski, B., Richie, J., Bailen, M., Shute, J., and Anderson, J. (2013). Map projection on the web (POW). *44th LPSC,* Abstract #2068.

Hargitai, H. (2014). Patera. *Encyclopedia of Planetary Landforms*, Springer, New York.

(2007) PIA09257: Io in motion. *NASA Planetary Photojournal*. *Online*. *http://photojournal.jpl.nasa.gov/catalog/PIA09257*. Accessed 27 Jan 2016.

Jaeger, W.L., Turtle, E.P., Keszthelyi, L.P., Radebaugh, J., McEwen, A.S., and Pappalardo, R.T. (2003). Orogenic tectonism on Io. *Journal of Geophysical Research, 108 (E8),* 12-1-12-18.

Johnson, T.V., Cook, A.F., Sagan, C., and Soderblom, L.A. (1979). Volcanic resurfacing rates and implications for volatiles on Io. *Nature, 280,* 746-750.

Jozwiak, L.M. (2014). Constraining the lithospheric thickness of Io from a modified heat-pipe model. *45th Lunar and Planetary Science Conference*, Abstract #1160.

Kargel, J.S., Delmelle, P., and Nash, D.B. (1999). Volcanogenic sulfur on Earth and Io: Composition and spectroscopy. *Icarus, 142 (1)*, 249-280.

Keszthelyi, L. and McEwen, A. (1997). Magmatic differentiation of Io. *Icarus, 130*, 437-448.

Keszthelyi, L.P., McEwen, A.F., and Taylor, G.J. (1999). Revisiting the hypothesis of a mushy magma ocean in Io. *Icarus, 141*, 415-419.

Keszthelyi, L.P., Jaeger, W.L., Turtle, E.P., Milazzo, M., and Radebaugh, J. (2004). A post-Galileo view of Io's interior. *Icarus, 169 (1)*, 271-286.

Kirchoff, M.R., McKinnon, W.B., and Schenk, P. (2003). Spherical harmonic analysis of mountain and volcanic center distribution on Io. *American Geophysical Union Fall Meeting*. Abstract #P41A-0399.

Kirchoff, M.R., and McKinnon, W.B. (2005). Mountain building on Io: An unsteady relationship between volcanism and tectonism. *36th Lunar and Planetary Science Conference*. Abstract #2245.

Kirchoff, M.R. and McKinnon, W.B. (2009). Formation of mountains on Io: Variable volcanism and thermal stresses. *Icarus, 201*, 598-614.

Kirchoff, M.R., McKinnon, W.B., and Schenk, P. (2011). Global distribution of volcanic centers and mountains on Io: Control by asthenospheric heating and implications for mountain formation. *Earth and Planetary Science Letters, 301*, 22-30.

Leone, G., Wilson, L., Davies, A.G. (2011). The geothermal gradient of Io: Consequences for lithosphere structure and volcanic activity. *Icarus, 211*, 623-635.

Lopes, R.M.C., Kamp, L.W., Douté, S., Smythe, W.D., Carlson, R.W., McEwen, A.S., Geissler, P.E., Kieffer, S.W., Leader, F.E., Davies, A.G., Barbinis, E., Mehlman, R., Segura, M., Shirley, J., and Soderblom, L.A. (2001). Io in the near-infrared: Near-infrared mapping spectrometer (NIMS) results from the Galileo flybys in 1999 and 2000. *Journal of Geophysical Research, 106 (E12)*, 33053-33078.

Mann, P. (2007). Global catalogue, classification, and tectonic origins of restraining- and releasing bends on active and ancient strike-slip fault systems. *Geological Society of London Special Publication*, *290,* 13-142.

Masursky, H., Schaber, G.G., Soderblom, L.A., and Strom, R.G. (1979). Preliminary geological mapping of Io. *Nature, 280,* 725-729.

McEwen, A.S. and Soderblom, L.A. (1983). Two classes of volcanic plumes on Io. *Icarus, 55,* 191-217.

McEwen, A.S., Matson, D.L., Johnson, T.V., and Soderblom, L.A. (1985). Volcanic hot spots on Io: Correlation with low-albedo calderas. *Journal of Geophysical Research, 90 (B14),* 12,345-12,379.

McEwen, A.S., Lunine, J., and Carr, M.H. (1989). Dynamic geophysics of Io, *Time-Variable Phenomena in the Jovian System, NASA Special Publication, NASASP-464,* 11-47.

McEwen, A.S., Keszthelyi, L., Spencer, J.R., Schubert, G., Matson, D.L., Lopes-Gautier, R., Klaasen, K.P., Johnson, T.V., Head, J.W., Geissler, P., Fagents, S., Davies, A.G., Carr, M.H., Breneman, H.H., and Belton, M.J.S. (1998). High-temperature silicate volcanism on Jupiter's moon Io. *Science*, *281,* 5373, 87-90.

McEwen, A.S., Belton, M.J.S., Breneman, H.H., Fagents, S.A., Geissler, P., Greeley, R., Head, J.W., Hoppa, G., Jaeger, W.L., Johnson, T.V., Keszthelyi, L., Klaasen, K.P., Lopes-

Gautier, R., Magee, K.P., Milazzo, M.P., Moore, J.M., Pappalardo, R.T., Phillips, C.B., Radebaugh, J., Schubert, G., Schuster, P., Simonelli, D.P., Sullivan, R., Thomas, P.C., Turtle, E.P., and Williams, D.A. (2000). Galileo at Io: Results from High-Resolution Imaging. *Science*, *288*, 1193-1198.

McKinnon, W.B., Schenk, P.M., and Dombard, A.J. (2001). Chaos on Io: A model for formation of mountain blocks by crustal heating, melting, and tilting. *Geology, 29 (2),* 103-106.

Milazzo, M. (2000). Rifting at Hi'iaka Patera?. *PIRL,* University of Arizona, *Online*. https://pirlwww.lpl.arizona.edu/wiki/missions/Galileo/releases/19May_i25hiiaka. Accessed 23 Jan 2016.

Morabito, L.A., Synnott, S.P., Kupferman, P.N., and Collins, S.A. (1979). Discovery of currently active extraterrestrial volcanism. *Science, 204 (4936),* 972.

Nash, D.B., Yoder, C.F., Carr, M.H., Gradie, J., and Hunten, D.M. (1986). Io. *Satellites*, University of Arizona Press, Tucson, 629-688.

O'Reilly, T. C. and Davies, G.F. (1981). Magma transport of heat on Io: A mechanism allowing a thick lithosphere. *Geophysical Research Letters, 8 (4),* 313-316.

Peale, S.J., Cassen, P., and Reynolds, R.T. (1979). Melting of Io by tidal dissipation. *Science, 203 (4383),* 892-894.

Perry, J., Lopes, R.M.C., Spencer, J.R., and Alexander, C. (2007). A summary of the *Galileo* mission and its observations of Io. *Io After Galileo*, Springer, Chichester, UK, 35-59.

Radebaugh, J., Keszthelyi, L.P., McEwen, A.S., Turtle, E.P., Jaeger, W., and Milazzo, M. (2001). Paterae on Io: A new type of volcanic caldera?. *Journal of Geophysical Research, 106 (E12),* 33,005-33,020.

Radebaugh, J. (2005). Formation and evolution of paterae on Jupiter's moon Io. Doctoral Dissertation, University of Arizona, Tucson, AZ.

Radebaugh, J., Schleiffarth, K., and Christiansen, E.H. (2011). Internal stresses of Io are revealed by surface lineations. *42nd Lunar and Planetary Science Conference*, Abstract #2755.

Ross, M.N., Schubert, G., Spohn, T., and Gaskell, R.W. (1990). Internal structure of Io and the global distribution of its topography. *Icarus, 85,* 309-325.

Sagan, C. (1979). Sulphur flows on Io. *Nature, 280,* 750-753.

Schaber, G.G. (1982). The geology of Io. *The Satellites of Jupiter*, University of Arizona Press, Tucson, AZ, USA, 556-597.

Schenk, P.M. and Bulmer, M.H. (1998). Origin of mountains on Io by thrust faulting and large-scale mass movements. *Science, 6 (5356),* 1514-1517.

Schenk, P.M. and Hargitai, H. (1998). Morphology and distribution of mountains on Io. *Bulletin of the American Astronomical Society, 30,* Abstract #1121.

Schenk, P., Hargitai, H., Wilson, R., McEwen, A., and Thomas, P. (2001). The mountains of Io: Global and geological perspectives from Voyager and Galileo. *Journal of Geophysical Research, 106 (E12),* 33,201-33,222.

Schubert, G., Stevenson, D.J., and Ellsworth, K. (1981). Internal structure of the Galilean satellites. *Icarus, 47,* 46-59.

Segatz, M., Spohn, T., Ross, M.N., and Schubert, G. (1988). Tidal dissipation, surface heat flow, and figure of viscoelastic models of Io. *Icarus, 75,* 187-206.

Smith, B.A., Soderblom, L.A. Johnson, T.V., Ingersoll, A.P., Collins, S.A., Shoemaker, E.M., Hunt, G.E., Masursky, H., Carr, M.H., Davies, M.E., Cook, A.F.II, Boyce, J., Danielson, G.E., Owen, T., Sagan, C., Beebe, R.F., Veverka, J., Strom, R.G., McCauley, J.F., Morrison, D.,

Briggs, G.A., and Suomi, V.E. (1979). The Jupiter system through the eyes of Voyager I. *Science, 204 (4396),* 951-972.

Spencer, J.R., Stern, S.A., Cheng, A.F., Weaver, H.A., Reuter, D.C., Retherford, K., Lunsford, A., Moore, J.M., Abramov, O., Lopes, R.M.C., Perry, J.E., Kamp, L., Showalter, M., Jessup, K.L., Marchis, F., Schenk, P.M., and Dumas, C. (2007). Io volcanism seen by New Horizons: A major eruption of the Tvashtar volcano. *Science, 318 (5848),* 240-243.

Spotila, J.A., Farley, K.A., and Sieh, K. (1998). Uplift and erosion of the San Bernardino Mountains associated with transpression along the San Andreas Fault, California, as constrained by radiogenic helium thermochronometry. *Tectonics, 17 (3),* 360-378.

Strom, R.G., Terrile, R.J., Hansen, C., and Masursky, H. (1979). Volcanic eruption plumes on Io. *Nature, 280,* 733-736.

Tackley, P.J., Schubert, G., Glatzmaier, G.A., Schenk, P., Ratcliff, J.T., and Matas, J. (2001). Three-dimensional simulations of mantle convection in Io. *Icarus, 149*, 79-93.

Tu, R. (2015). A study of the parametric and nonparametric linear-circular correlation coefficient. *California Polytechnic State University,* San Luis Obispo, 1-24.

Turcotte, D.L. and Schubert, G. (2002). *Geodynamics, 2nd ed*. John Wiley & Sons, New York, USA, 456.

Turtle, E.P., McEwen, A.S., Keszthelyi, L.P., and Schenk, P.M. (1999). Formation and evolution of Ionian mountains. *30th Lunar and Planetary Science Conference,* Abstract #1971.

Turtle, E.P., Jaeger, W.L., Keszthelyi, L.P., McEwen, A.S., Milazzo, M., Moore, J., Phillips, C.B., Radebaugh, J., Simonelli, D., Chuang, F., Schuster, P., and the Galileo SSI Team (2001). Mountains on Io: High-resolution Galileo observations, initial interpretations, and formation models. *Journal of Geophysical Research, 106 (E12),* 33,175-33,199.

Turtle, E.P., Jaeger, W.L., and Schenk, P. (2007). Ionian mountains and tectonics: Insight into what lies beneath Io's lofty peaks. *Io After Galileo*, Springer, Chichester, UK, 109-131.

Veeder, G.J., Matson, D.L., Johnson, T.V., Blaney, D.L., and Goguen, J.D. (1994). Io's heat flow from infrared radiometry: 1983-1993. *Journal of Geophysical Research, 99 (E8),* 17095-17162.

Veeder, G.J., Matson, D.L., Johnson, T.V., Davies, A.G., and Blaney, D.L. (2004). The polar contribution to the heat flow of Io. *Icarus, 169,* 264-270.

Veeder, G.J., Davies, A.G., Matson, D.L., and Johnson, T.V. (2009). Io: Heat flow from dark volcanic fields. *Icarus, 204,* 239-253.

Veeder, G.J., Davies, A.G., Williams, D.A., Matson, D.L., Johnson, T.V., and Radebaugh, J. (2011). Io: Heat flow from dark paterae. *Icarus, 212,* 236-261.

Williams, D., Schenk, P.M., Moore, J.M., Keszthelyi, L.P., Turtle, E.P., Jaeger, W.L., Radebaugh, J., Milazzo, M.P., Lopes, R.M.C., and Greeley, R. (2004). Mapping of the Culann-Tohil region of Io from Galileo imaging data. *Icarus, 169*, 80-97.

Williams, D.A. and Howell, R. (2007). Active volcanism: Effusive eruptions. *Io After Galileo*, Springer, Chichester, UK, 133-161.

Williams, D.A., Keszthelyi, L.P., Crown, D.A., Yff, J.A., Jaeger, W.L., Schenk, P.M., Geissler, P.E., and Becker, T.L. (2011). Volcanism on Io: New insights from global geologic mapping. *Icarus, 214*, 91-112.

Williams, D., Keszthelyi, L.P., Crown, D.A., Yff, J.A., Jaeger, W.L., Schenk, P.M., Geissler, P.E., and Becker, T.L. (2012). Geologic Map of Io. *U.S. Geological Survey Scientific Investigations,* Map 3168, scale 1:15,000,000.

Wise, D.C. (1963). Keystone faulting and gravity sliding driven by basement uplift of Owl Creek Mountains, Wyoming. *AAPG Bulletin, 47(4)*, 586-598.

Yoder, C.F. (1979). How tidal heating in Io drives the Galilean orbital resonance locks. *Nature*, *279*, 767-770.

Zhukov, Y.M. (2010). Applied spatial statistics in R. *Online*. Available: http://www.people.fas.harvard.edu/~zhukov/Spatial4.pdf. Accessed 27 Jan 2016.